

International Journal of Coal Science & Technology

Analysis of a rock slope instability mechanism combining wedge and circular failure in a soft rock mass

--Manuscript Draft--

Manuscript Number:		
Full Title:	Analysis of a rock slope instability mechanism combining wedge and circular failure in a soft rock mass	
Article Type:	S.I. : Soft Rock Engineering Challenge and Innovations	
Funding Information:	Ministerio de Ciencia e Innovación (PID2024-156154OB-I00)	Dr. Leandro R. Alejano
	China Sponsorship Council (202406560041)	Mr Sifan Yuan
	China Sponsorship Council (202306410072)	Mr. Bingdong Ding
	Consellería de Cultura, Educación e Ordenación Universitaria, Xunta de Galicia	Dr. Ignacio Pérez-Rey
Abstract:	<p>One of the most common failure mechanisms in rock slope stability analysis is wedge failure, where sliding of an element of a rock mass occurs along two pre-existing discontinuities, whose intersection daylight on the slope face. The kinematic analysis of this mechanism prescribes that failure can only take place when the intersection of both discontinuities at stake dips less than the slope face. However, when the intersection line of a wedge dips slightly more than the slope face, a modified version of this mechanism can occur. In this paper, the authors describe in detail an actual case study of this type of failure mechanism that occurred in a 25-m high, 38°-dipping bench of an abandoned open-pit mine in Spain. To illustrate how this phenomenon indeed takes place, a timeline description of events, intact rock and rock mass characterization and a detailed slope failure analysis are included. Moreover, indicative limit equilibrium and more accurate numerical modelling approaches are presented guiding how to estimate factors of safety (FoS) against this complex type of instability mechanisms. Furthermore, some situations associated with soft rock where these and similar slope failure mechanisms could take place are discussed. These approaches can be of help for the purpose of back analyzing similar case studies and for designing slopes when potential failures of this type are prone to occur.</p>	
Corresponding Author:	Leandro R. Alejano University of Vigo: Universidade de Vigo SPAIN	
Corresponding Author Secondary Information:		
Corresponding Author's Institution:	University of Vigo: Universidade de Vigo	
Corresponding Author's Secondary Institution:		
First Author:	Sifan Yuan, master in geologocal Engineering	
First Author Secondary Information:		
Order of Authors:	Sifan Yuan, master in geologocal Engineering	
	Bingdong Ding	
	Kai Guan, Ph.D. in Mining Engineering	
	Ignacio Pérez-Rey, Ph.D. Mining Engineering	
	Tonglu Li	
	Leandro R. Alejano	
Order of Authors Secondary Information:		

Author Comments:	Following an invitation of Professor Luís Ribeiro de Sousa we decided to submit it to the special issue on soft rock engineering of your reputed journal, so it can be additionally presented in the ISRM Workshop on Soft Rocks to be held in Porto, Portugal, 15-16 May 2025.
Opposed Reviewers:	
Manuscript Classifications:	40: Coal mining; 50: Rock mechanics/ground control
Additional Information:	
Question	Response

Analysis of a rock slope instability mechanism combining wedge and circular failure in a soft rock mass

Sifan Yuan¹, Bingdong Ding^{1,2}, Kai Guan^{1,3}, Ignacio Pérez-Rey¹, Tonglu Li⁴, Leandro R. Alejano^{1*}

¹ CINTECX, Universidade of Vigo, GESSMin Group, Department of Natural Resources and Environmental Engineering, Galicia 36310, Spain

² Department of Engineering Geology and Geotechnical Engineering, China University of Geosciences, Wuhan 430074, China

³ Center for Rock Instability and Seismicity Research, School of Resource and Civil Engineering, Northeastern University, Shenyang 110819, China

⁴ School of Geological Engineering and Geomatics, Chang'an University, Xi'an 710054, China

* Corresponding author: alejano@uvigo.gal

ABSTRACT

One of the most common failure mechanisms in rock slope stability analysis is wedge failure, where sliding of an element of a rock mass occurs along two pre-existing discontinuities, whose intersection daylight on the slope face. The kinematic analysis of this mechanism prescribes that failure can only take place when the intersection of both discontinuities at stake dips less than the slope face. However, when the intersection line of a wedge dips slightly more than the slope face, a modified version of this mechanism can occur. In this paper, the authors describe in detail an actual case study of this type of failure mechanism that occurred in a 25-m high, 38°-dipping bench of an abandoned open-pit mine in Spain. To illustrate how this phenomenon indeed takes place, a timeline description of events, intact rock and rock mass characterization and a detailed slope failure analysis are included. Moreover, indicative limit equilibrium and more accurate numerical modelling approaches are presented guiding how to estimate factors of safety (FoS) against this complex type of instability mechanisms. Furthermore, some situations associated with soft rock where these and similar slope failure mechanisms could take place are discussed. These approaches can be of help for the purpose of back analyzing similar case studies and for designing slopes when potential failures of this type are prone to occur.

Key-words: Slope stability, Combined failure mechanisms, Wedge-circular failure, Soft rock

1 Introduction

The fundamentals of rock slope engineering were mainly developed by John Bray, Evert Hoek and Ted Brown in the sixties of the past century, financed by mining companies and based on some preliminary works. This background knowledge was reported in the book “Rock Slope Engineering” by Hoek & Bray (1974). After this milestone, some relevant improvements have been developed up to the present day. These include, to cite the most relevant achievements, the statement and development of rock mass classification systems, the improvement of intact rock, joint and rock mass mechanical characterization techniques and their estimates based on field and lab approaches, the improvement and coding of factor of safety (FoS) computations for different failure mechanisms, the development and application to rock

slope stability of different families of numerical models and the recent relevant improvements in advanced surveying and monitoring methods.

From a geomechanical point of view, Hoek & Bray (1974) and other rock slope stability basic texts (Wyllie & Mah 2004; Kliche 1999; González de Vallejo et al. 2002; Ramírez-Oyanguren & Alejano 2008) define four typical failure mechanisms identified in rock slope instability phenomena and comprehending planar failure, wedge failure, toppling failure and circular or rotational failure. In this way, even today, when designing an open pit mine slope or a rock cut in a road, these are the potential failure mechanisms that are typically analyzed. Only sometimes, wall slope failure mechanisms (Walton & Atkinson 1979; Stead & Eberhardt 1997; Alejano et al. 2011; Havaej et al. 2014) are also analyzed.

Based on the so-called kinematic analysis, and stereographic representation of discontinuities measured in the field, the type or types of failure mechanisms potentially occurring in a rock slope can be identified (Hoek & Bray 1974). Once recognized, limit equilibrium method (LEM)-based analytical techniques can be applied to estimate the factor of safety (FoS) for each type of failure mechanism as presented in the above-mentioned general textbooks and other documents focusing problem solving and case studies (Hoek 2000; Harrison & Hudson 2000; Alejano 2014). Computer codes that implement these LEM solutions are currently available (Rocscience 2023a, b, c & d), facilitating the calculation of the FoS for every case at stage. Additionally, they implement ad-hoc techniques such as sensitivity analysis or statistical approaches to account for the impact of the natural variability of the geomechanical and geometric parameters in the slope stability computations.

Some studies have put forward complex slope stability problems in open pit coal mines (Walton & Atkinson 1978; Stead & Eberhardt 1997; Alejano et al. 2011; Zhao et al. 2020; Yang et al. 2023), often related to the presence of soft rocks including coal or coal measures in the slopes at stake and the occurrence of complex failure instability mechanism in line with the approach presented in this study.

A good number of instability cases reflected in the scientific literature and observations in human-made slopes put forward that slope instability phenomena cannot always be clearly classified within these four types of simple failure mechanisms. In this regard, it is interesting to look at the database of rock slope failures compiled by Bar & Barton (2024), where about 8 % are qualified as unknown failures and, interestingly, only 6 % are attributed to circular failure mechanisms, which implies that circular failures may not be so common in slopes excavated in rock. However, in practical engineering, a good number of failure instabilities are attributed to this type of mechanism, so it seems that engineers tend to back-analyze these cases by obtaining values of cohesion and friction that indicate failure for the prescribed geometrical and water conditions, and often use these parameters to redesign slopes, without paying sufficient attention to the actual failure mechanism at stake.

More complex mechanisms take place in rock slopes, which can often be qualified as failure associated with a combination of typically two, or sometimes more, of these simple failure mechanisms. Based on the last author's personal experience (Alejano et al. 2010; Alejano et al. 2012; León-Buendía et al. 2014; Alejano et al. 2019) and on a literature review on combined failure mechanisms (Coulthard et al. 2004; Böhme et al. 2013; Mohtarami et al. 2014; Gu and Huang 2016; Amini and Ardestani 2019; Xia et al. 2019; Gong et al. 2023; Wei et al. 2024; Cui et al., 2025), it seems that a good number of actual failures

in rock slopes, maybe up to 20 % based on the authors' personal record of cases, are due to the combination of simple failure mechanisms. To identify these combined failure mechanisms, it is necessary to have a good knowledge of the joint patterns of the rock masses and carefully observe the ultimate geometry of failures in-place.

To address this problem in a more rigorous manner, it is interesting to assess all the potential possible combinations of two of the four simple failure mechanisms traditionally accounted for in rock slope engineering, and considering the location of the mechanism, i.e., in the upper or in the lower part of the slope. This is illustrated in Fig. 1, where the proposed naming includes both the names of the simple failure mechanisms separated by a hyphen, naming in first place the one occurring in the rear upper part of the slope. A few papers reported, in a more or less inadvertently manner, rock slope failure cases associated with combined failure mechanisms, which are usually described under different definitions and names. We can mention cases of toppling-circular (Alejano et al. 2010; Mohtarami et al. 2014; Xia et al. 2019), planar-circular (Walton & Atkinson 1979; Havaej et al. 2014), or circular-toppling (Alejano et al. 2012; Amini & Ardestani 2019) among others.



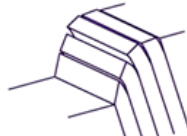

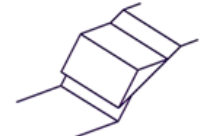
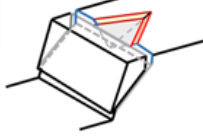
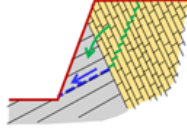
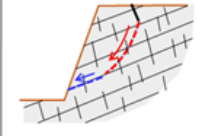

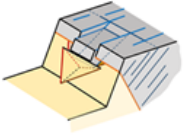
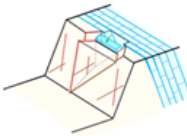
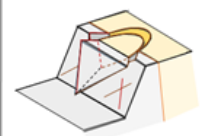
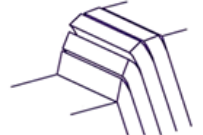

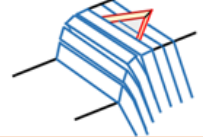
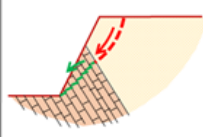

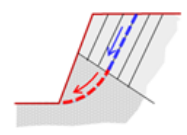
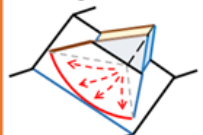
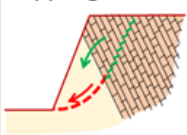
Combined mechanism failures in rock slopes					
UP DOWN	PLANAR	WEDGE	TOPPLING	CIRCULAR	
					
	X	Wedge-Planar 	Toppling-Planar 	Circular-Planar 	
	Planar-Wedge 	X	Toppling-Wedge 	Circular-Wedge 	
	Planar-Toppling 	Wedge-Toppling 	X	Circular-Toppling 	
	Planar-Circular 	Wedge-Circular 	Toppling-Circular 	X	

Fig. 1 Graphical table showing all possible 12 combinations of two (out of the four) simple rock slope failure mechanisms occurring in the upper and lower part of the slope, respectively. A wedge-circular failure is studied in this article, marked in the orange rectangle. Contributing to the advance in the identification and analysis of the potential occurrence and stability level of every type of these possible failure combinations is within the ultimate aims of this study.

108 It seems that some potential combinations, such as toppling-circular, can be more common than others,
109 such as wedge-planar. But this is something that would require first some thinking on geometrical
110 considerations, and then, years of observation and reporting of case studies. In the meantime, it would
111 be a good policy to find and analyze in due detail actual failures observed in rock slopes, where a
112 combination of simple failure mechanisms can be identified.

114 To contribute to this endeavor, the authors present and analyze in this study a rock slope failure that took
115 place after heavy rains in a revegetated bench of an old lignite open-pit mine in northwest Spain, where
116 a wedge-circular failure mechanism in a tectonized and weathered soft phyllite rock mass was eventually
117 identified. To do that, some considerations relevant to the wedge-circular combined failure mechanism
118 will first be presented. Then, the failure will be described in terms of observations in place, underlying
119 geology, previous excavations, and the characterization of the rock mass where it took place.

121 The rock mass and joint sets observed were characterized in situ and by means of lab tests, and the
122 relevant geomechanical parameters were then estimated. Finally, the observed failure mechanism was
123 analyzed, first based on indicative simplified planar approaches and then, by means of a 3D DEM
124 numerical model, which was eventually able to reproduce in a reasonably representative manner the
125 failure observed in the field.

127 This combined wedge-failure mechanism seems to be behind potential open pit slope failures, as
128 addressed in recent studies (Rogers et al. 2023; Cui et al. 2025). The first reference states that many
129 multi-bench-scale blocks formed in large open pit mines comprise non-daylighting wedges that are often
130 stable because they occur behind or beside a buttress of rock mass that stabilizes the block, rendering the
131 simple kinematic solution ineffective. However, when these wedges occur in soft rock or poor-quality
132 rock masses, they can become unstable. So, the type of mechanism studied here tends to be particularly
133 relevant in large slopes of open pit mines and in slopes in soft rock masses.

135 **2 Background of study area**

137 **2.1 The *As Pontes* open-pit mine**

139 The *As Pontes* mine was located in *As Pontes de García Rodríguez, A Coruña*, in the northwest of Spain
140 (Fig. 2a). Fig. 2b shows the location of the *As Pontes* mine, which covered an area of 24 km² (3 km x 8
141 km) and reached a maximum depth of 230 m. The open-pit lignite operation, carried out by ENDESA (a
142 Spanish electricity company), commenced in 1976 and continued until 2007. Over its operational lifespan,
143 the mine produced approximately 270 million t of lignite, making it one of Spain's largest lignite sources
144 and a key contributor to the country's electricity generation during the late 20th century.

146 After the cessation of mining activities, the pit underwent a controlled flooding process that lasted six
147 years, resulting in the formation of a large lake, which was fully established by 2013. This lake now
148 occupies the former excavation site, transforming the area into a post-mining landscape (Fig. 2d).
149 Although the slopes of the mine were overall stable after the mine pit was impounded, a localized small-
150 size instability phenomenon affecting an area of roughly 1900 m² was observed on the northern slope
151 (Fig. e). This instability is analysed in due detail in this study.

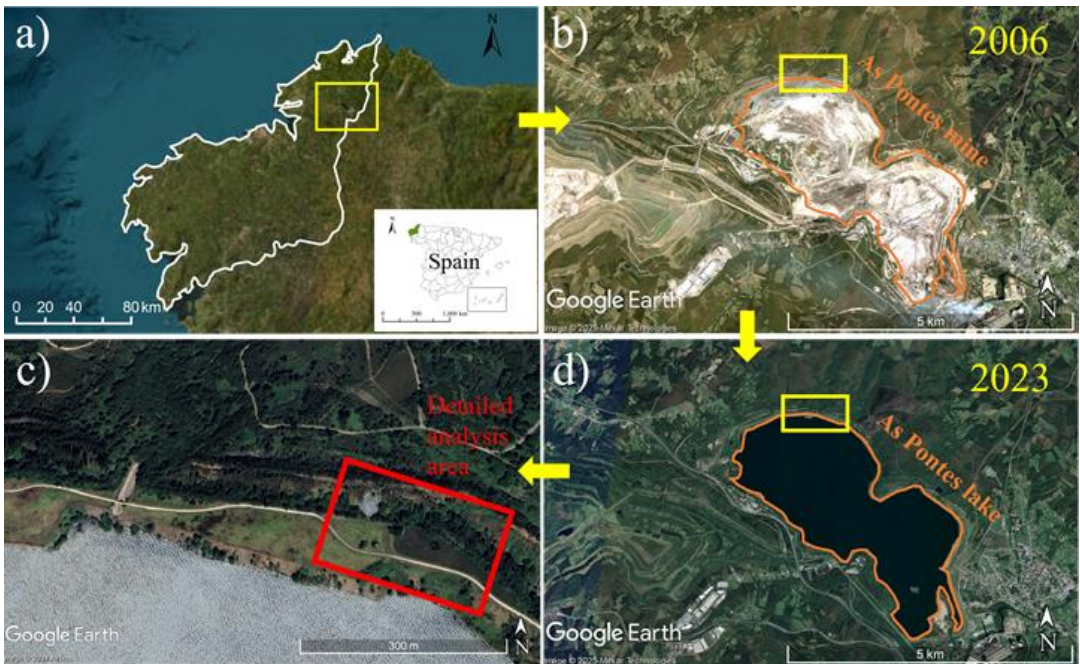


Fig. 2 General schematic and aerial photographs of the Mine: **a)** Location in Spain, **b)** Pre-closure aerial view, **c)** Detailed study area of local instability in 2017, and **d)** Aerial view once the mine was fully flooded.

2.2 Basic geology

The geology of the region is associated with the Variscan orogeny, which at large scale produced igneous rock batholiths surrounded by metamorphic rocks with different arrangements. A large-scale view of the geology of the area is illustrated in Fig. 3. These orogenic materials later suffered various geological processes.

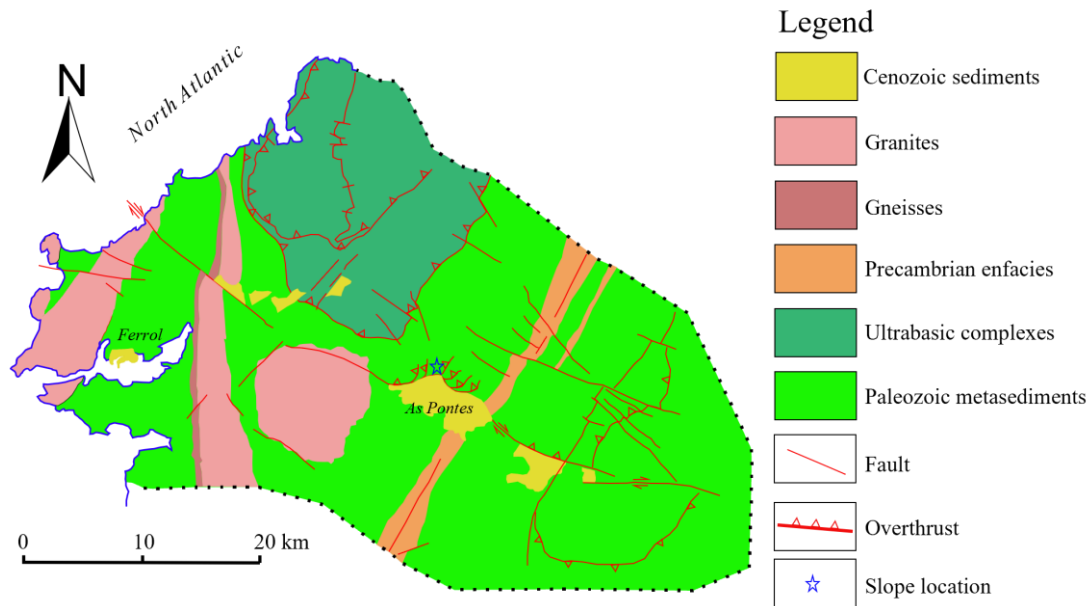


Fig. 3 Geological and structural map at large scale of the study area. The As Pontes mine basin, represented in yellow color, can be observed in the middle of the map. Modified from Ferrus Piñol (1994).

The lignite deposit at the mine of *As Pontes* occurs in a pull-apart basin. A basin is a zone where subsidence generates accommodation space for the deposition of sediments. A pull-apart basin is a structural basin where two overlapping (*en échelon*) strike-slip faults create an area of crustal extension undergoing tension, which causes the basin to sink down. Frequently, the basins are rhombic or sigmoidal in shape (Frish et al. 2010).

In the current case, a zone formed by granite batholiths and metamorphic rocks due to the Variscan Orogeny in the late Paleozoic, cooled and became brittle so cracks in NW-SE and WSW-ENE formed (Fig. 4a). The shear horizontal and, also vertical, movements of these faults in local zones generated pull-apart basins during the Mesozoic, associated with movements of blocks (Fig. 4b). This shear movement also produced thrusting in the weaker meta-sedimentary rocks identified as phyllite as illustrated in Fig. 4c. One of these basins is the one at *As Pontes*, which is a good example of gentle restraining bend (Ferrus-Piñol, 1994), which was later filled with clay and organic matter during the Cenozoic (Fig. 4d) generating the lignite deposit, later mined at *As Pontes* (Monge, 1987). The damage associated with thrust faulting, particularly in the northern part of the basin, strongly tectonized metamorphic rocks, particularly around the failure under scrutiny. This tectonic damage significantly lowers the quality of the rock mass, something that can greatly influence excavation response (Buergi et al. 1999).

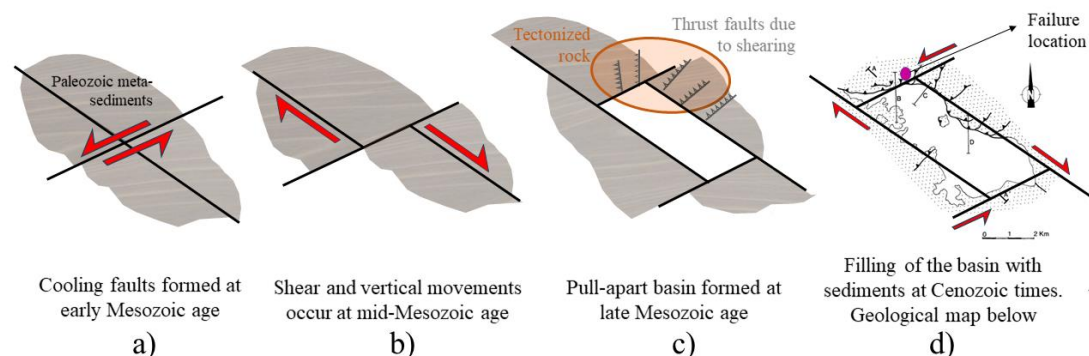


Fig. 4 Formation of a pull-apart basin a) faulting, b and c) movement and opening of the basin and d) filling of the basin with sediments including clay and organic matter to ultimately produce lignite. Remark that, the northern part of the basin is tectonized due to thrusting occurred in parallel with the shearing movements while formation of the valley later filled with clays and organic matter.

Therefore, *As Pontes* valley corresponds to a pull-apart basin filled with Cenozoic sediments including clay and lignite, which was the mineral exploited in the open pit. The original valley is located in Ordovician phyllitic rocks within a northern strike-slip fault system, associated with a double restraining-bend geometry of NW-SE master dextral strike-slip fault.

The main geological formations in the zone are Paleozoic meta-sediments, with phyllite and schist being the predominant rocks. The localized instability affected a poor-quality rock mass in moderately weathered phyllite, mobilizing several hundred cubic meters of rock. The occurrence of discontinuities, coupled with weathering of the rock mass and water pressures during periods of heavy rainfall, likely contributed to producing the localized slope failure.

2.3 Field characterization

Two field visits were conducted in 2021 to investigate the localized instability in the upper part of the north slope of the mine. The unstable section, composed of weathered and tectonized phyllite (Fig. 5g), is approximately 35 m long, with a slope height of 25 m, a dip direction of 189°, and a dip of 38°. Different pictures of the instability zone are presented in Fig. , where a central sketch synthesizes the most relevant observations.

Figs. 5h and 5i provide frontal and top views of the instability. The slide mass has accumulated in the middle and lower parts of the slope, and a distinct two-wedge saw-tooth-shaped back limit of the failure is clearly visible at the crown of the slope. To enhance clarity, a simplified line drawing in the middle of the figure outlines the key instability features. In the rock mass and mostly at the accessible part at the top of the slope, three major discontinuity sets were identified: S_0 , J_1 , and J_2 . S_0 represents the foliation and primary weakness direction of the phyllite, while J_1 and J_2 are additional joint sets. The main sliding surfaces are formed by S_0 and J_1 , creating two dihedral sliding planes (Figs. 5b and 5d) with a central protuberance (Fig. 5e). The right-side sliding surface is defined by joint J_1 presenting a large outcropping area after failure (Fig. 5g). J_2 , with a sub-parallel strike to the slope and a dip against it, has apparently contributed to the formation of tension cracks at the crest (Fig. 5a).

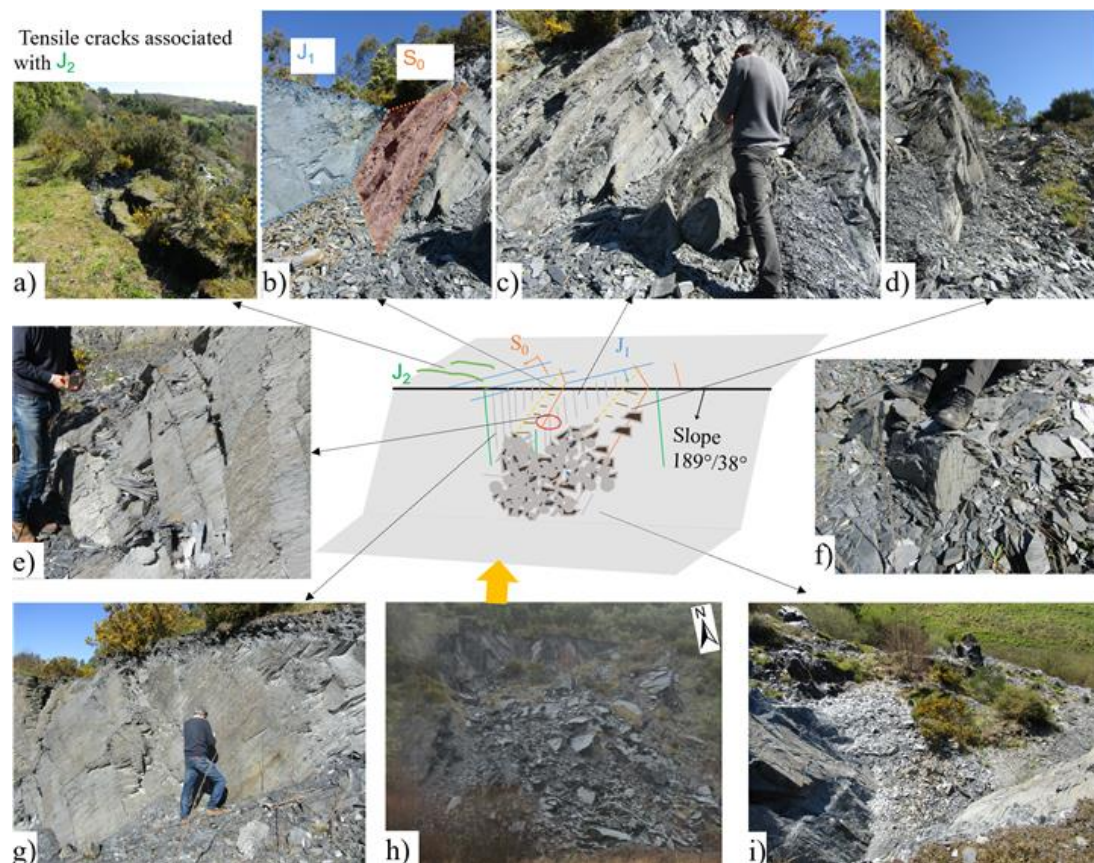


Fig. 5 Illustrations and photos of the main features of the failed slope sketched in the center of the figure: **a)** Tensile cracks associated with J_2 **b)** Wedge-shaped sliding surface formed by S_0 and J_1 **c)** Protuberant rock mass formed by S_0 and J_1 **d)** Sliding surface on the upper left side **e)** Detail of S_0 **f)** Low-quality tectonized rock mass in the accumulation body **g)** Sliding surface along J_1 **h)** Front view **i)** Overhead view from above

A small number of discontinuities were characterized in the phyllite outcrop of the fallen area, due to its limited size. Fig. 6 illustrates the stereographic projections of the discontinuity poles measured in the field, while Table 1 summarizes their average orientation values together with their more relevant geomechanical features.

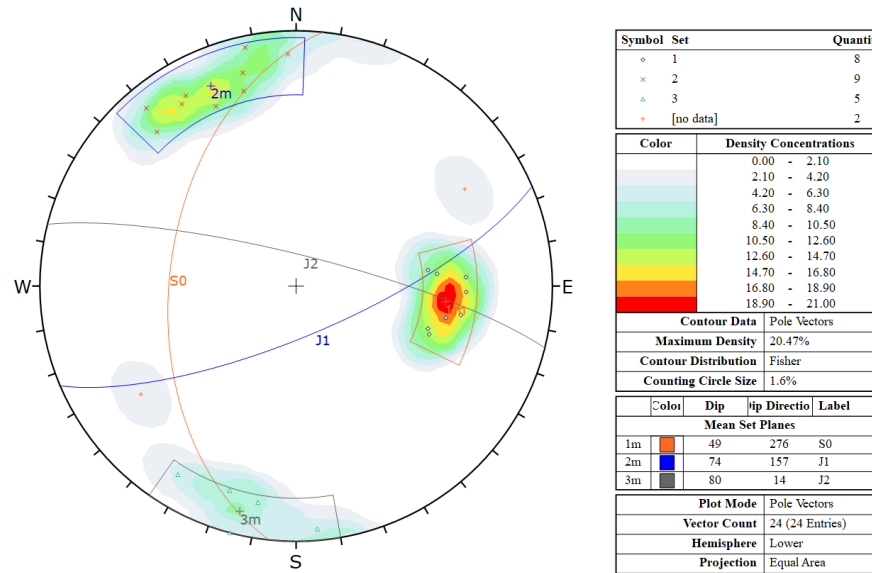


Fig. 6 Equal area lower hemispherical stereographic representation of the poles of the representative planes of each discontinuity set, along with iso-distribution lines of poles and estimation of the mean orientations of each discontinuity set

Table 1 Summary of survey results for joint sets

Joint set			S ₀	J ₁	J ₂
Number of joints measured			8	7	5
Dip-direction (°)			276	157	14
Dip (°)			49	74	80
Continuity Strike (m)			>20	10-20	10-20
Spacing (m)			0.1	0.5	>2
JRC	Range		3-5	5-11	5-11
	Mean		3.5	8.1	6.2
Schmidt hammer reb.	Range		10-20	10-28	18-30
	Mean		15.8	19	20
JCS (MPa)	Range		18-32	18-42	28-56
	Mean		25.4	28.4	37.5
Weathering degree			II-III	II-III	II-III
Water			Slightly wet	Wet	Slightly wet

2.4 Laboratory tests

A small number of rock samples were collected in place with the aim of characterizing the main intact rock parameters. Due to the fracturing of the rock, it was generally difficult to collect large elements of rocks and prepare standard size samples in sufficient number, so the authors generally resorted to small samples and indirect determination of rock parameters.

Laboratory tests on phyllite samples included density tests, point load tests, tilt tests, and slake durability

tests following the testing guidelines of the International Society for Rock Mechanics and Rock Engineering (ISRM 2007). Fig. 7 shows the samples used to perform the above-mentioned tests. The rock density as measured in the laboratory was 2 800 kg/m³. Point load tests indicate that the unconfined compressive strength exhibits significant anisotropy according to the direction of the applied force in relation to the foliation or cleavage. The average derived unconfined compressive strength is 22 MPa when the load is applied parallel to the foliation, and 58 MPa when applied perpendicular to the foliation. Based on these values, an unconfined compressive strength of no less than 22 MPa is considered for estimation. Tilt tests on non-weathered flat rock surfaces determined that the dry basic friction angle was approximately 26.7°. The slake durability tests indicated a moderate susceptibility to weathering, with a durability index (Id₂) of 98.63%.

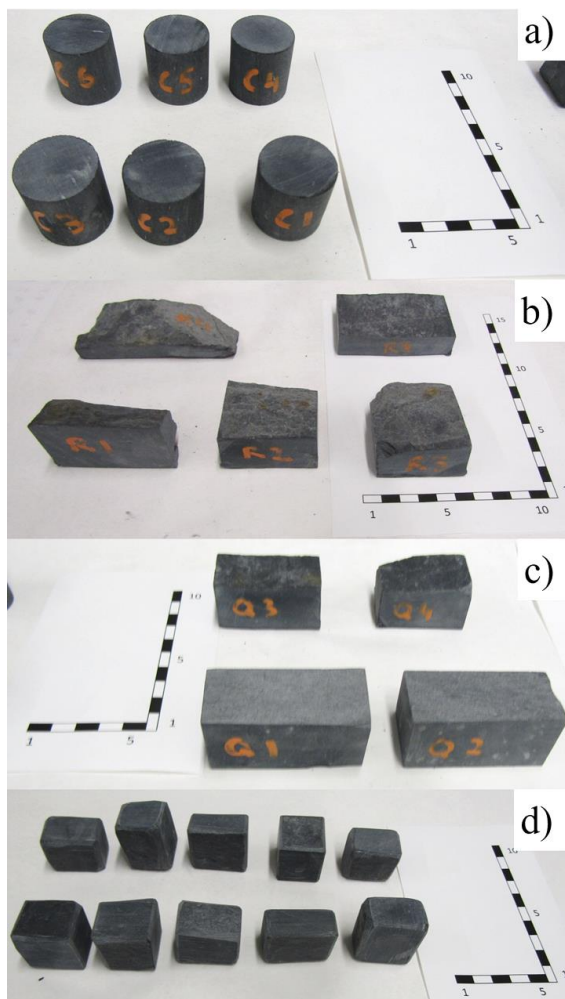


Fig. 7 Different samples obtained and tested: **a)** Cylindrical samples for point load tests, **b)** Fragment samples for point load test, **c)** Parallelepiped fragments for tilt test, and **d)** Small cuboid samples used for the slake durability tests.

2.5 Geotechnical properties of the rock mass and rock joints

Based on field and laboratory data, and following the classification of Bieniawski (1979), a rock mass rating (RMR) of 40 was obtained. The obtained RMR value of 40 indicates a medium to poor-quality rock mass. This helps to have an overall understanding of the rock mass quality, also providing a basis for estimating the geotechnical properties of the rock and joints, which are presented in Table 2.

Table 1 The geotechnical properties of the rock and joints

	Parameter	Value
Rock	Density(kg/m ³)	2 800
	Rock mass modulus (GPa)	0.7-2.8
	UCS(MPa)	22-58
	<i>m_i</i>	5-9
	GSI	32-38
	D	0.7-1
	Friction (°)	17.9-39.8
	Cohesion (kPa)	57-195
	Friction (°)	16-20
	Cohesion (kPa)	1-3
Joint	Shear stiffness (GPa/m)	1

The rock mass has an unconfined compressive strength (UCS) ranging from 22 to 58 MPa, reflecting variations in material strength. Following Hoek et al. (2002) and taking into account the blocky rock mass structure and poor surface conditions, the Geological Strength Index (GSI) was estimated to range between 32 and 38 with an average of 35 based on the approaches proposed by Cai et al. (2004) and Truzman (2017), specially focusing metamorphic rocks. This range suggests a tectonically fractured and moderately weathered rock mass. The *m_i* parameter, which characterizes rock frictional strength behavior, was considered within the range of 5 to 9, based on tests carried out by the authors in similar phyllite rocks of the region. The disturbance factor (D) was deemed to vary between 0.7 and 1, indicating different levels of excavation-induced damage depending on the type of excavation (ripping or use of blasting in some parts of the slope).

Based on the above range of Hoek-Brown parameters, the estimated GSI values and the height of the slope, equivalent Mohr-Coulomb parameters were calculated (Hoek et al. 2002). The friction angle of the rock mass would range from 17.9° to 39.8°, and the cohesion from 57 kPa to 195 kPa, reflecting a relatively large range of shear strength properties potentially influenced by weathering and fracturing. For the estimation of the rock mass deformation modulus (*E_m*), Equation (1) proposed by Hoek et al. (2002) was used. The value of *E_m* was assumed to range between 0.8 GPa and 2.5 GPa.

$$E_m (\text{GPa}) = \left(1 - \frac{D}{2}\right) \sqrt{\frac{UCS}{100}} \cdot 10^{((GSI-10)/40)} \quad (1)$$

In a first approach, authors have resorted to the so-called Barton-Bandis approach to estimate the potential actual shear strength of the discontinuities involved in the instability case studied (Barton & Choubey 1977; Barton & Bandis 1990) considered as scale-affected shear strength of rough, weathered, and unfilled wet discontinuities. The application of this approach for *S₀* and *J₁*, based on the field geomechanical characterization and accounting for residual friction angle, effect of wetness and potential failure geometries provided values of cohesion and friction in the range 2-4 kPa and 20-24°.

However, previous studies carried out for mine management, based on back analysis of slope stability in

tectonized weathered phyllite materials use strength parameter of cohesion 2 kPa and friction 18° to successfully model this type of slope made of materials as that found in the current case. Since these parameters are in the same range as those estimated based on field characterization, and they were shown to be able to reproduce the actual behavior of slopes at a larger scale they were considered as realistic average strength parameters potentially representative of the joints affecting the failure under scrutiny. Potential ranges of variability based on calculations above will range in $c = 1\text{--}3$ kPa and $\phi = 16\text{--}20^\circ$.

Since the shear stiffness of the joint is significantly influenced by size effects, it was set to 1 GPa/m, while the normal stiffness was assumed to be ten times the shear stiffness. These values represent significantly softer mechanical properties compared to the intact rock. These parameters, which are not necessary for carrying out limit equilibrium method (LEM)-based approaches, can be important when carrying out numerical models of slopes in order to assess the overall slope stability and potential failure mechanisms.

3 Failure mechanism description

3.1 Failure evolution based on Google Earth images

Fig. 8a shows the appearance of the failure under scrutiny photographed from the base of the slope in 2021, where discontinuity planes are observable at the top. Fig. 8b provides an aerial perspective of this unstable area, taken from a Google Earth image in 2017, where discontinuities and two tension cracks can also be identified at the top. Although discontinuities are present, a clear or straightforward failure pattern cannot be readily identified, nor is there evidence of a simple slope failure mechanism, such as planar, wedge, circular, or toppling failure, is observed in this case.

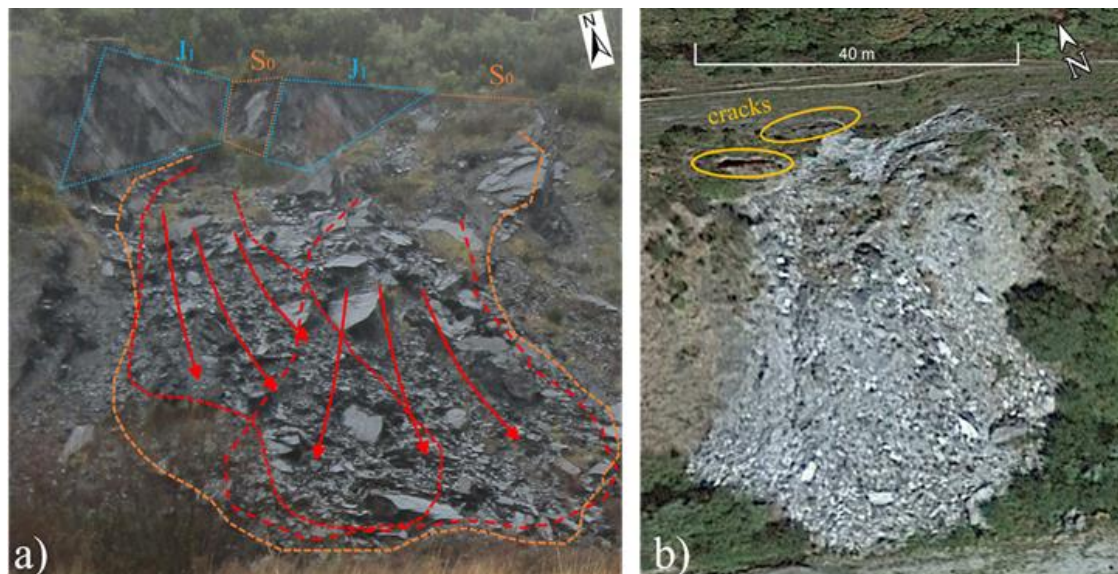


Fig. 8 a Photograph from the base of the slope showing the instability of the bench, and **b** Detailed aerial photograph of the local instability taken from Google Earth in October 2017

To better understand the failure mechanism, a series of temporal images from Google Earth were

analyzed. These images, covering an area of approximately $300 \text{ m} \times 150 \text{ m}$ (marked by the red rectangle in Fig. 2c), are shown in Figs. 9a–9d. By examining these images, it is possible to reconstruct the gradual development of instability and gain insight into its initiation and propagation over time, and to determine the potential trigger.

Considering the start of the open pit mining exploitation in 1976 and the subsequent mine planning, it is estimated that the study area was probably excavated in the 1980s. By 2003 (Fig. 9a), the area had already been excavated, and a 25-m high bench with a 38° slope was left in the north-western portion of the image, which remained stable at the time of the image (2003). In the central part of the image, a similar bench was left, which experienced some type of instability and was stabilized with a riprap retaining wall, as can be seen in Fig. 9a, marked with a red ellipse, and subsequent images.

Fig. 9b shows the same area in 2009, after the mining extraction process had stopped but before the lake filling was completed. By this time, the entire area was revegetated, with denser vegetation in the previously mentioned retaining wall. No signs of instability are observed. Thus, no stability problems were identified in the detailed analysis area more than 25 years after excavation.

The following aerial image (Fig. 9c) was taken in March 2015, six years after the previous one and about three years after the lake filling was completed. By this time, vegetation had become denser, and localized erosion was observed on the south-east due to stream evolution. Nevertheless, more than 30 years after excavation, no significant instability phenomena had occurred in the studied zone, despite fluctuations in groundwater levels associated with occasional periods of intense rainfall.

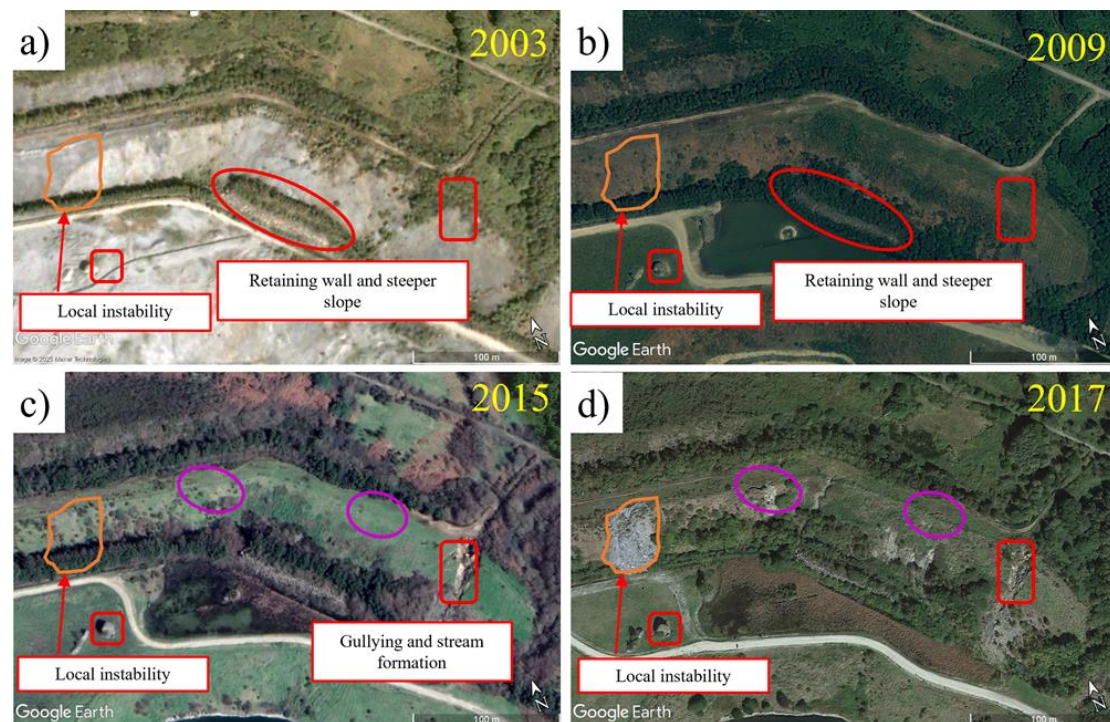


Fig. 9 Details of the instability area in a) 2003, b) 2009, c) 2015, and d) 2017

The aerial image in Fig. 9d, taken in October 2017 shows, for the first time, the appearance in Google Earth of the local instability under study. There has been no notable change in the state observed in this photograph compared to the field observations made during visits in early 2021. Additionally, the opening of two local tension cracks at the top of the bench can be observed, marked with magenta ovals.

Although the exact date of the occurrence of the instability phenomenon is unknown, it must have occurred between March 2015 and October 2017 (the dates of the images before 9c and after 9d the event). A date could be around the first months of 2016, which were among the rainiest winter months in Galicia and particularly in the mine area of this century (Fig. 10). During this time, various minor instability phenomena were reported in quarry benches and road slopes in Galicia, northwest Spain. Regardless of the exact date, probably around 35 years passed since the opening of the area until the occurrence of this local instability.

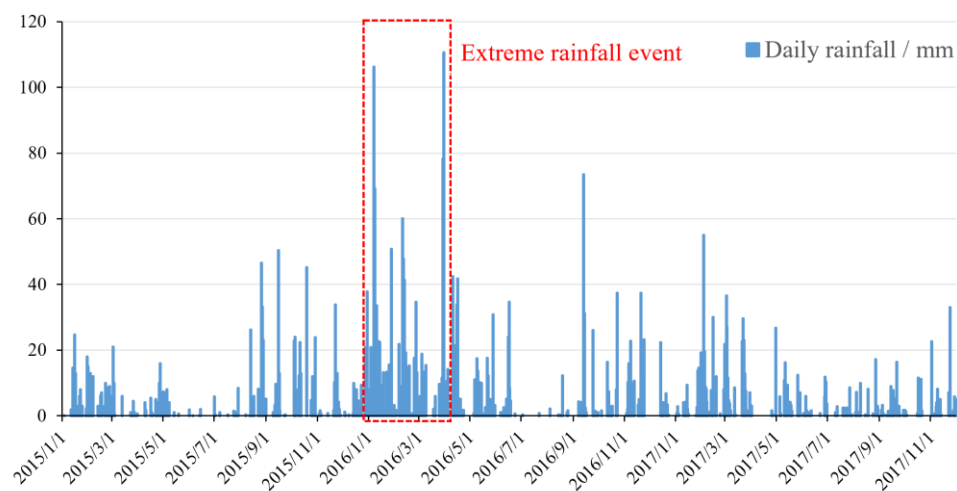


Fig. 101 Daily rainfall during the period of time when the slope might fail, *A Coruña* observatory, 45 km from the slope area

Field investigations during two visits to the area and the observation of aerial photographs at various times rule out any relationship with instability phenomena of the general north slope of the mine. Instead, it is just a local failure with no significant impact on the overall slope stability. This local instability is attributed to progressive rock weathering processes, ultimately exacerbated by high water pressures during intense precipitation events. This behaviour aligns with natural erosive processes that commonly induce localized failures in natural slopes and road cuts, particularly during prolonged or extreme rainfall conditions.

3.2 Failure mechanism identification

To identify the possibility of this type of failure mechanism, we compare the orientation of the bench slope under study with the stereographic representation of the discontinuity orientations measured in the field, as shown in Fig. 11. For a better understanding, the interpretation of the failure mechanisms is presented with front and side view sketches in Fig. 12. As illustrated, a double-wedge rock block is

formed by the dihedral planes of S_0 and J_1 . The intersection (I) of these planes dips at an angle greater than 40° , which means it cannot intersect (daylight) the slope face dipping 38° .

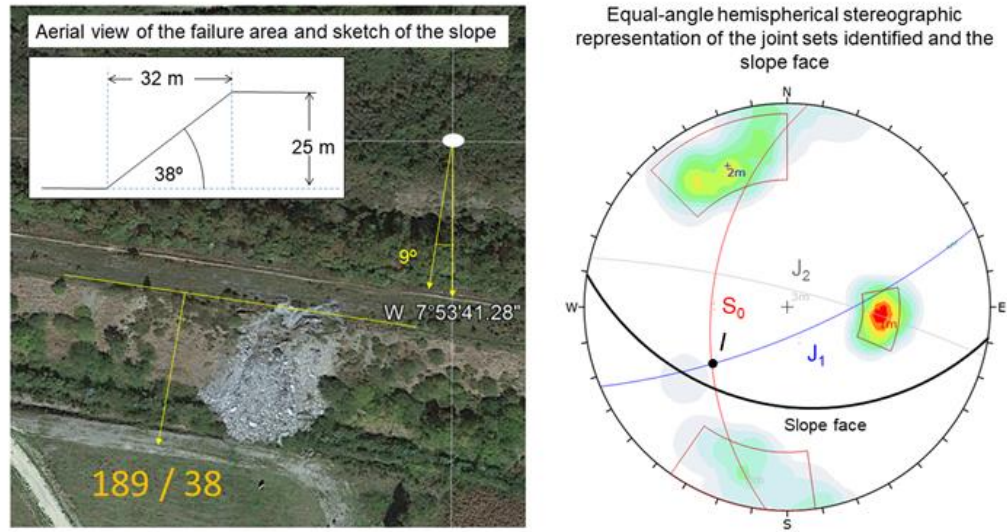


Fig. 112 Aerial view of the failed bench and stereographic representation of the joint sets at stake and the slope face.

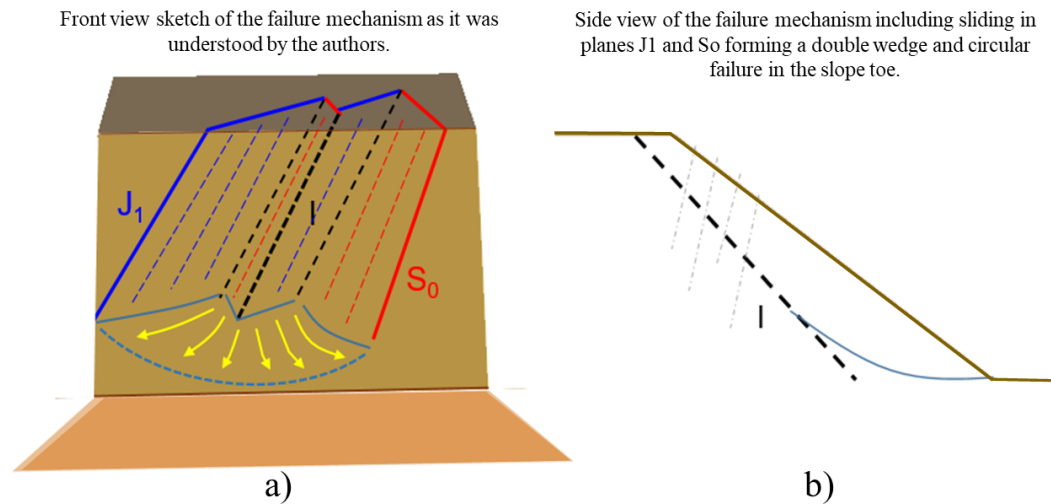


Fig. 12 Interpretation of the failure mechanisms showed in a) front view and b) side view schematics.

Consequently, no wedge failures occur under these conditions. However, as the authors interpret, if there was a possible shear zone through the toe of the slope breaking through the rock mass, the failure mechanism could involve a typically circular failure pattern in this part. Based on these observations, and considering the relatively low quality of the rock mass and its susceptibility to weathering processes, the so-called wedge-circular instability mechanism was introduced to explain the phenomenon of combined wedge and circular failure mechanisms in soft rocks. Although it may be claimed to be speculative, this reasoning is consistent with all the field observations and will be further evaluated using

simplified planar methods and 3DEC numerical modeling to verify its validity.

4 Back-Analysis Using the Simplified Planar Approach and 3DEC Approach

In this section, the authors analyze the failure of the slope from a rock engineering point of view. First a simplified 2D geometry plane strain limit equilibrium approach considering a planar-circular failure is applied. Then a 3D numerical DEM approach considering a wedge-circular failure is presented, representing more soundly in the geometry and rock engineering behavior of the observed failure.

4.1. Simplified planar approach

The Limit Equilibrium Method (LEM) allows failure analysis by assuming predefined or potential failure surfaces and uniform stress distributions. They deliver reasonably easy estimations of the Factor of Safety (FoS), provided the failure mode is previously identified. Moreover, they facilitate back-analysis and statistical approaches, which tend to be more cumbersome to carry out in the context of numerical approaches. SLIDE 2 (Rocscience 2023c) is a 2D limit equilibrium slope stability program for circular or non-circular failure surfaces in soil or rock slopes. The model proposed here represents a planar-circular failure, substituting sliding in 4 planes (Fig. 12) by sliding in one single plane, so the results are not expected to be accurate, because the actual geometry of failure is not properly represented, but they could be indicative of failure trends. The results are expected to be non-conservative, providing FoS somewhat smaller than the real ones.

A plane that contains the intersection line (I) of the wedge planes S_0 and J_1 while maintaining a strike parallel to the slope determines the orientation of the joint plane. Using stereographic projection, this plane is calculated to have a dip of 50° . Considering the continuity of discontinuities in the S_0 and J_1 sets, it can be estimated that this joint plane could have an average equivalent persistence of about 30 m and a dip of 50° . In the field failure, the sliding surfaces outcrops approximately 8 m behind the head of the original slope. A weak layer is used to represent the joint intersection by assigning the friction angle and cohesion estimated for the joints.

Based on the mentioned geometry and rock and joint parameters, three types of LEM based-analyses, including a deterministic analysis, a sensitivity analysis, and a probabilistic analysis, were conducted to investigate the wedge-circular instability mechanism in a 2D simplified manner.

4.1.1 Deterministic analysis

The shear strength of the basal plane is fixed on cohesion 2 kPa and friction angle 18° , as explained in section 2.5. Three deterministic analyses were performed varying the strength parameters of the rock mass. The first and second analyses correspond to the mean (typical values) and minimum strength values (highly weathered rock values), while the third represents an intermediate set of values between mean and minimum values. The first analysis is considered to roughly represent the state of the rock mass just after mine closure (no weathering), and the third one, the state after some relevant weathering took place, possibly representing the situation 40 years after the excavation of the bench in a weathered zone. The calculated factors of safety (FoS) for these cases under different groundwater conditions are presented in

Table 3. As observed, if the material is in its mean, as it should have been at the time of excavation of this bench about 30 years ago, the slope would be stable even when saturated ($FoS = 1.36$). At the minimum value, the material exhibits characteristics of strong tectonization and weathering, leading to slope failure under both dry ($FoS = 0.981$) and saturated ($FoS = 0.75$) conditions. For the intermediate material parameters under dry conditions, the slope remains stable with a FoS of 1.25; however, undergoing heavy rainfall and subsequent saturation, the FoS decreases to 0.976, indicating failure.

Fig.13 presents the failure mechanism of saturated intermediate values scenario ($Fos = 0.976$). The Spencer method identifies the failure surface as a combination of a 27.52 m planar segment and a circular component, with the circular part emerging at the toe of the slope. Considering the predefined geometry, the planar segment was initially set at 30 m, slightly longer than the computed 27.52 m. However, trial tests indicate that increasing the length of the planar segment beyond this value does not significantly affect the overall failure mechanism.

Table 3 Rock strength parameters and factors of safety for 2D deterministic analysis

Values	Friction (°)	Cohesion (kPa)	Water	FoS
Mean values	28.8	126	Dry	1.66
			Saturated	1.36
Minimum values	17.9	57	Dry	0.981
			Saturated	0.75
Intermediate values	24	75	Dry	1.25
			Saturated	0.976

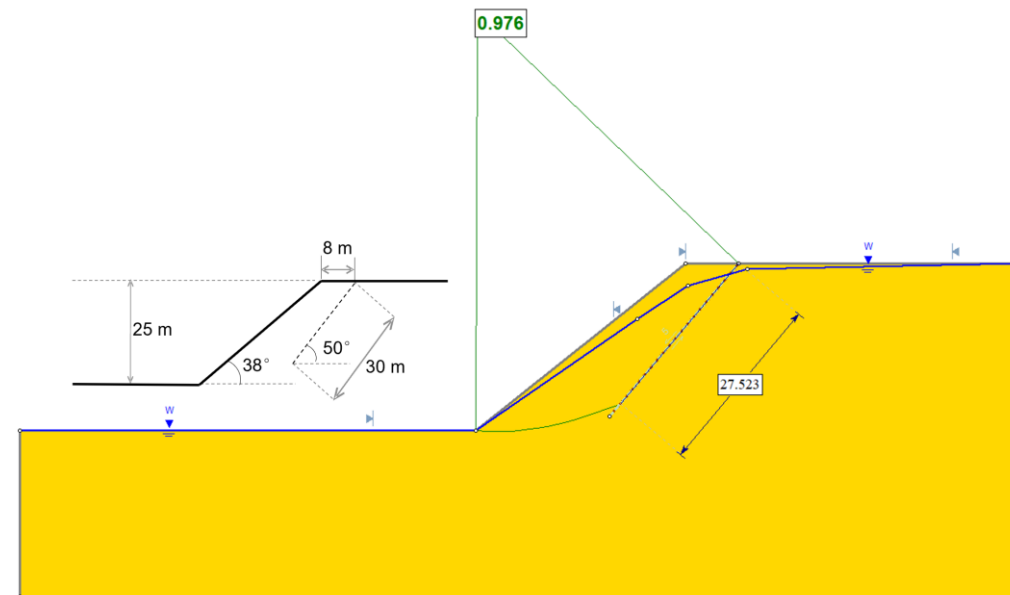


Fig.13 The interpretation of the failure surface for the saturated intermediate values scenario

4.1.2 Sensitivity analysis

To account for parameter uncertainty or variability in this study, the authors carried out a sensitivity

analysis based on the LEM approach. Individually analyzed input strength parameters were varied between 50% and 150% of their mean values, while the rest were kept constant at 100%. For the rock mass strength, the mean values (100%) correspond to the intermediate values case in Table 3. For the joint, the mean values (100%) are friction angle of 18° and cohesion of 2 kPa. For the water effect, the water table position 50% and 100% are at the middle and the highest point of the slope respectively. The percentage changes in input variables and their effects on the computed factors of safety are illustrated in the spider diagram shown in Fig. 14.

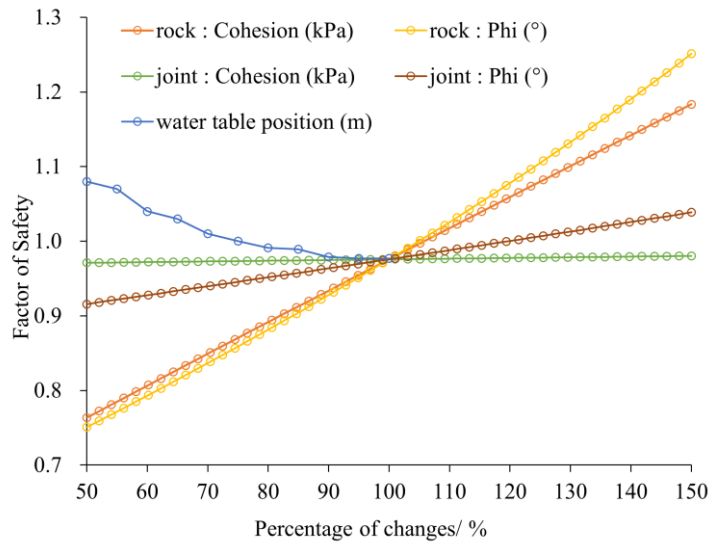


Fig. 14 Sensitivity analysis spider diagram.

Based on this variability assessment graph (Fig.14), rock mass strength and water table location play a critical role in the stability of the planar-circular mechanism. An increase in rock material strength generally enhances stability, whereas a higher water table significantly reduces the FoS due to increased pore water pressure and reduced effective stress. Conversely, joint properties have a comparatively lower impact on stability. Since the dip angle of the joint is greater than that of the slope, the downslope component of the driving force along the joint is relatively small. As a result, the joint strength (once fixed their orientation) does not play a relevant role on stability.

As shown in the previous analysis, failure occurred only when the rock material strength degraded to a critical level and at the same time the slope became fully or almost fully saturated. Moreover, failure was thought to occur when the poor-quality soft rock mass was rather weathered, and an extreme rainfall event took place for these conditions. These factors were the primary contributors to the occurrence of the wedge-circular instability mechanism.

4.1.3 Probabilistic analysis

A Probabilistic analysis was conducted to back-analyze the rock material properties that could contribute to instability by assigning statistical distributions to the Hoek-Brown parameters (UCS, GSI, D, and m_i). UCS uses triangular distribution to reflect the central tendency and range of its test data, while GSI, D,

and m_i use uniform distribution due to their more significant subjectivity, insufficient data, or difficulty in quantifying the distribution shape. The equivalent Mohr-Coulomb parameters were assumed to follow a triangular distribution. The statistical parameters used are summarized in Table 4, where the mean values represent the average expectable values of the parameters for the observed conditions, while the minimum and maximum values correspond to rock masses of lower and higher quality, respectively. Considering the highest water table position, the probabilistic analyses are presented in Fig. 15.

Table 4 Distribution characteristic of input rock and joint parameters in probability analysis

	Parameters	Distribution	Minimum value	Mean value	Maximum value
	UCS (MPa)	triangular	22	40	58
Rock mass	GSI	uniform	32	35	38
(Hoek-Brown)	m_i	uniform	5	7	9
	D	uniform	0.7	0.85	1
Rock mass	Friction (°)	triangular	17.9	28.8	39.8
(Mohr-Coulomb)	Cohesion (kPa)	triangular	57	126	195
Joints	Friction (°)	triangular	16	18	20
(Mohr-Coulomb)	Cohesion (kPa)	triangular	1	2	3

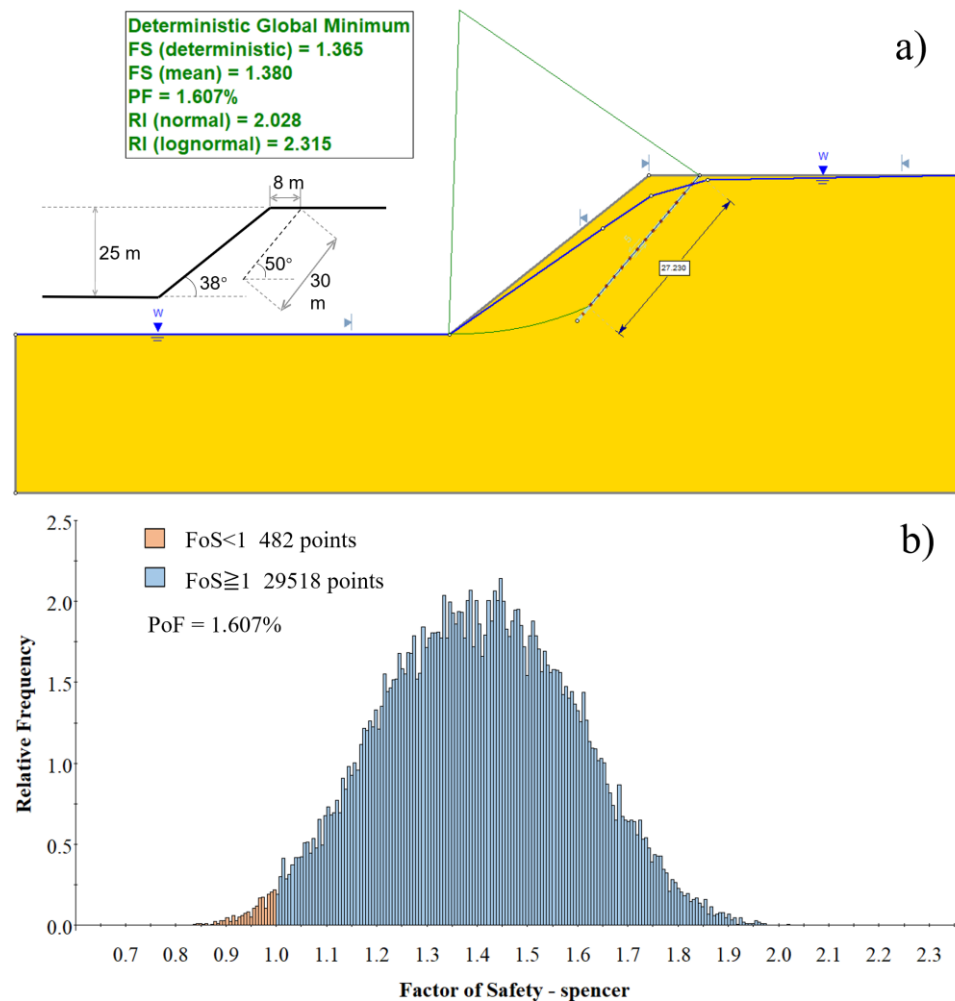


Fig. 15 a) The interpretation of the failure surface and probabilistic factor calculated from mean values **b)** Distribution of Factor of Safety

The probabilistic analysis estimated a probability of failure (PoF) = 1.607%, which falls within the acceptable range for open pit slopes. Indeed, 30 years after excavation, in the roughly 1.5 km long northern slope bench of the mine (Fig. 2c) no failure was observed (PoF = 0%). Only after around 35 years, a local failure was observed along a 35-m section of the bench, corresponding to a PoF of approximately 2.5% (35 m /1500 m).

As mentioned above, this approach would be non-conservative one providing FoS smaller than the actual ones. However, considering the lower strength parameters in the actual slope as the intermediate values, one can use this approach as a practical engineering tool to analyze and design the slope. This simplified plain strain analysis representing a planar-circular failure can be considered indicative of the instability situation of the slope, and it can be resorted to as a practical engineering tool when insufficient information of the failure mechanism is available. However, it does not represent the actual geometry of the phenomenon that took place, providing FoS smaller than the real ones (minimum dry would be unstable, while it is observed to be generally stable).

4.2 DEM Numerical modelling approach

As observed in the field, the two joint sets form a double wedge-shaped rock element, whose sliding surface is a spatial multi-plane. The orientation of each plane has an impact on its stability, and the simplified LEM-based approach presented above cannot accurately describe it, so a 3D discrete element method is convenient for a more rigorous and realistic analysis. The 3D discrete element method-based software 3DEC (Itasca 2019) is a code able to model the mechanical behavior of jointed rock masses and uses discrete blocks (rigid or deformable) and contacts to simulate complex failure mechanisms, including multi-planar and non-linear responses.

In order to calculate the level of safety by means of this or any other numerical code it is necessary to resort to the so-called shear strength reduction technique or SSRT (Dawson et al. 1999), which estimates a strength reduction factor (SRF), similar but not equal than a LEM-based FoS. To compute SRF, the code progressively reduces (or increases if unstable) all the strength parameters of a slope (joints, rock) by an evolving factor, and the stress analysis is computed. Different values of SRF are repeated automatically by the code until the model becomes unstable, so the analysis results do not converge (or become stable). In this way, the critical strength reduction factor SRF is computed. It is relevant to note that this SRF affects all materials in the model, even if they are not with the failed zones, whereas the LEM analytical FoS computed above (ratios stabilizing forces over destabilizing forces) refers to the stability of the predefined detachable element. In this way, if a situation of limit equilibrium occurs, FoS and SRF should both equal one. However, for rather stable or unstable situations, FoS and SRF may differ due to the different approaches used to compute them.

Using the 3DEC code, a model was set up including deformable blocks and joint plane contacts, as shown in Fig. 16. Displacements were restrained in the bottom and lateral sides of the model. The geotechnical parameters of rock and joint and contact parameters are presented in Table 5. Deformability joint parameters, including normal stiffness (Kn) and shear stiffness (Ks), should be carefully chosen. Joint shear stiffness (Ks) was established using Barton & Bandis's approach (1990) and the joint normal stiffness (Kn) value followed the relation suggested by Itasca (2019), considering the bulk and shear

modulus of the block material and the smallest size of the zone. The 3DEC analysis considered the strength parameter values used in the above LEM analysis, under both saturated and dry conditions. Likewise, the water table in the 3DEC model is set to match that in LEM analysis.

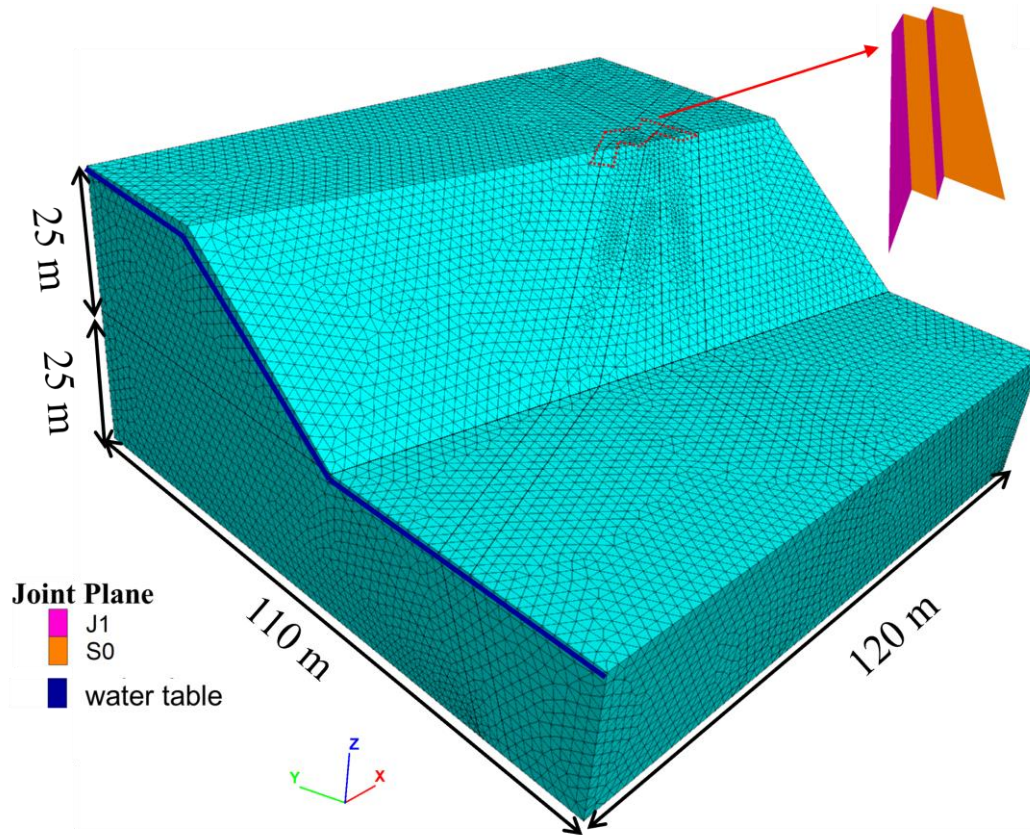


Fig. 16 Model features and dimensions used for 3DEC analysis

Table 5 Geotechnical parameters of rock mass and joint used in 3DEC analysis

Properties	Rock mass		Joint
Density (kg/m ³)	2 800		-
Bulk modulus (GPa)	3		-
Shear modulus (GPa)	1		-
Friction (°)	mean	28.8	18
	minimum	17.9	
Cohesion (kPa)	mean	126	2
	minimum	57	
Normal stiffness (GPa/m)	-		10
Shear stiffness (GPa/m)	-		1

A total of three analyses, accounting for different rock mass strength condition combinations, were analyzed. These analyses, along with the corresponding calculated SRF values, are presented in Table 6. Compared to LEM, the 3DEC analysis indicates greater stability under the same material strength, something the authors attribute to the more realistic geometry of the numerical approach, in such a way that the confinement of the potentially sliding element makes it slightly more stable if compared to plane strain conditions.

Table 6 3DEC analyses and calculated SRF

Values	Rock mass		Joint		Water	SRF
	Friction	Cohesion/	Friction	Cohesion/		
Mean values	28.8	126	18	2	Dry	2.10
					Saturated	1.71
Intermediate Values	24	75	18	2	Dry	1.60
					Saturated	1.24
Minimum values	17.9	57	18	2	Dry	1.26
					Saturated	0.96

The scenario representing the mean rock mass strength and non-weathered state after excavation produces a SRF value of 2.1 under dry conditions and 1.71 under saturated conditions. This supports the reasonability of the bench remaining stable for more than 30 years after excavation. Then, the same intermediate strength parameter scenario as in the LEM analysis was used, resulting in an SRF of 1.60 under dry conditions and 1.24 under saturated conditions, indicating again stability in both cases, unlike for the LEM approach. Finally, the scenario representing the minimum rock material strength, associated high tectonization and weathering of the rock mass, produces a SRF value of 1.26 under dry conditions, indicating stability, as generally observed in the zone even today, and 0.96 under saturated conditions, indicating failure for the possible conditions under which the observed failure took place (heavy rains fallen in the zone in early 2016). The geometry of the failure analyzed with 3DEC presented in Figure 17 and the estimated parameters represent more reliably the instability phenomenon that occurred in the zone under study.

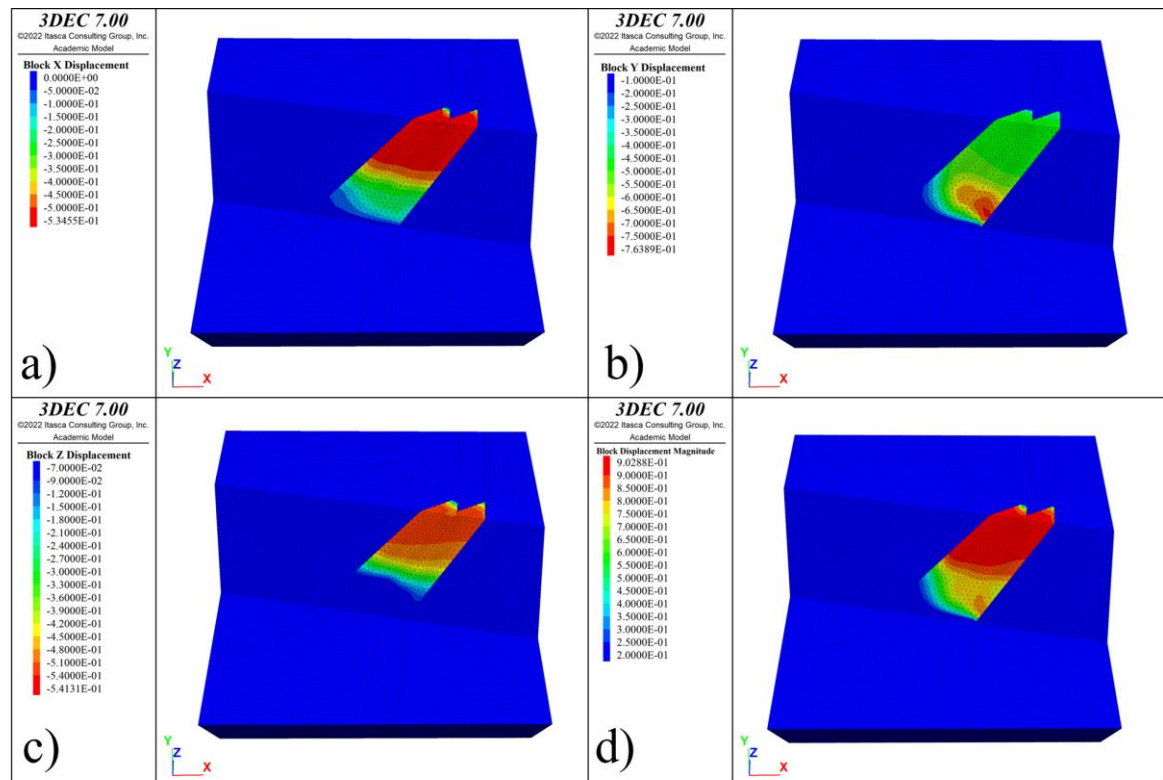


Fig. 17 3DEC analysis: displacement distribution for the case of minimum strength values and saturated slope. a) x-

direction, **b**) y-direction, **c**) z-direction, and **d**) magnitude

Fig. 17 shows the displacement distribution of the unstable state (minimum values saturated). As can be observed, the displacement consists of two components: the upper part exhibits a uniform displacement pattern, suggesting a wedge failure mechanism, while the lower part displays an uneven displacement distribution, characteristic of a circular failure mechanism.

5 Discussion

This study investigates a wedge-circular failure mechanism in an abandoned mine bench, offering insights into combined failure mechanisms in soft rock. On the one hand, the back-analysis using the simplified planar approach helps to understand the mechanism and roughly quantify the relevancy of the rock joint and rock mass strength parameters that may lead to failure. The sensitivity analysis highlights that rock mass strength and water pressure associated with water table position are the dominant factors influencing the stability of the slope. The simplified planar probabilistic analysis quantifies the probability of failure (PoF) by accounting for the distribution of strength parameters, providing a comprehensive understanding of the conditions under which instability occurs. However, the consideration of a planar failure proves to be unconservative, since it indicates failure for strength parameters probably somewhat over the actual ones at the time of failure. This is associated with the non-accurate geometry of failure considered.

On the other hand, back-analysis using the Shear Strength Reduction Technique (SSRT) and 3DEC numerical modeling confirms that this failure mechanism comprises two distinct components: 1) wedge sliding along discontinuities in the upper section, and (2) circular shear failure in the lower part of the slope outcropping near its toe. The 3D numerical model results represent well the failure mechanism observed, starting from the computed parameters based on field and laboratory data and rock engineering estimates and the water conditions at stake.

The findings of this study are consistent with previous research on similar failure mechanisms. Lo & Feng (2014) investigated a soft rock slope where the foliation was inclined parallel to the slope, exhibiting planar-circular deformation characteristics. Their parametric study highlighted that rock material strength, foliation strength, and foliation inclination are the most critical factors influencing the deformation of slate.

Rogers et al. (2023) describe two types of instability that are closely related to the mechanism considered in this study. The first one involves non-daylighting wedge in open pit mines, where instability is influenced by the front buttress rock properties of the rock element potentially unstable. The second type is controlled by the combination of structural features and rock mass strength, leading to a more complex failure mechanism. These two forms of instability align with what we defined as a combined instability mechanism, characterized by a failure process that incorporates both wedge and circular failure.

Cui et al. (2025) investigated a wedge-circular failure in an open-pit coal slope, where the wedge-shaped landslide body in the upper and middle sections of the slope slid downward, exerting pressure on the toe, which subsequently failed through a sheared area daylighting at the slope toe. This study highlights the interaction between wedge sliding and rotational failure, further supporting the concept of a combined

failure mechanism observed in this research.

Although a limited number of similar cases have been reported to date, both our research and the few cases available in the existing literature indicate that wedge-circular or planar-circular failure are primarily controlled by a combination of rock mass strength and structural characteristics. However, the dominant factors influencing failure vary across different cases, depending on geological, geotechnical and meteorological conditions. Given this variability, sensitivity analysis proves to be an effective approach for identifying the key parameters that govern slope stability and failure mechanisms in every case, and it can also be of help for design purposes.

In addition to material and structural controls, external triggers such as rainfall and human activities have been identified as key factors that could initiate failure. While in this case study, weathering and rainfall were the main trigger, Cui et al. (2025) identified rock mass damage due to blasting as a potential ultimate cause of instability in the case they studied.

6 Conclusions

This study investigated the factors contributing to a localized instability observed in the upper bench of the north slope of a closed lignite mine in Spain. Comprehensive field investigations were conducted to characterize the geotechnical conditions, supplemented by aerial photograph analysis and basic rock mechanics testing on in-situ recovered phyllite samples. The collected data allowed for the estimation of discontinuity orientations and their key geotechnical properties. The rock mass was characterized in terms of quality ranges, accounting for the tectonic damage suffered by the rock and weathering. Through the analysis of Google Earth images, the failure evolution was reconstructed, and a possible occurrence time was estimated.

The failure mechanism analyses revealed that the observed instability resulted from sliding along dihedral surfaces formed by the S_0 and J_1 discontinuity planes, with failure propagating through the rock mass via a circular shear rupture at its base. Unlike conventional failure mechanisms, this instability phenomenon exhibits a combined wedge and circular failure process, referred to in this study as *wedge-circular failure*. To the best of the authors' knowledge, this mechanism has rarely been reported in literature, partly due to the difficulty of its identification and partly because it may not be a very common occurrence. To assess slope stability, both a simplified plane-strain LEM-based approach and a more realistic 3DEC numerical modeling method were employed to estimate stability levels in terms of LEM factors of safety (FoS) and numerically obtained strength reduction factors (SRF) for this complex failure mechanism.

The deterministic analysis of the simplified planar approach was conducted to evaluate the FoS of rock mass parameters representing different degrees of weathering after mine excavation. This analysis identified the rock mass strength and water table position that may lead to failure. The sensitivity analysis further emphasized that rock mass strength and groundwater level are the primary factors influencing stability. A simplified plane-strain equivalent probabilistic analysis was conducted to evaluate the FoS distribution under variable input parameters and to determine the corresponding probability of failure

(PoF). The results are indicative, but not too accurate, due to the poor representativeness of the actual geometry of failure geometry. They suggest, though, that such failures would occur only under highly unfavorable geometric conditions, significant rock mass weathering, and extreme external factors. Simplified models like this, although not very accurate, can be a practical engineering tool when no other methods are available.

The more accurate 3DEC numerical model represents the geometry of the failure more reliably and suggests that the failure took place in a highly weathered area of the bench. This explains why, over the past decades, only a single occurrence of this failure mechanism has been recorded along the 1.5 km stretch of the northern slope of the closed open pit mine.

The results of this study additionally suggest that this type of combined failure mechanism is prone to occur in soft rock-mass environments where discontinuities do not fully penetrate the slope or where their strength or persistence is insufficient to induce failure on their own. In such cases, the soft rock mass provides partial resistance to instability. However, as the strength of the soft rock is not adequate to maintain long-term stability, failure may eventually occur through circular shear or creep deformation at the toe of the weak rock slope.

The presented results try to ultimately contribute to extending the database of instability rock slope case studies associated with combined failure mechanisms. This could be of help to attract the attention of practice rock engineers to consider these mixed failure modes when designing rock slopes in road cuts, quarries and open pit mines.

Acknowledgements: The authors acknowledge the Spanish Ministry of Science, Innovation & Universities for funding the project awarded under Contract Reference No. PID2024-156154OB-I00, partially financed by means of ERDF funds from the EU. The first author Sifan Yuan is grateful for the China Scholarship Council (CSC) for his stay at the University of Vigo by means of a CSC grant number 202406560041. The co-author Bingdong Ding is grateful for the Major Program of the National Natural Science Foundation of China (Grant No. 42090055) and China Scholarship Council (CSC) for his stay at the University of Vigo by means of a CSC grant number 202306410072. The co-author Ignacio Pérez-Rey acknowledges Xunta de Galicia for financing his research through a grant contract aimed at facilitating the postdoctoral training stage at the University of Vigo.

Author Contributions: Sifan Yuan: Writing – Original Draft, Formal Analysis. Bingdong Ding: Formal Analysis, Visualization. Kai Guan: Writing – Review & Editing. Ignacio Pérez-Rey: Investigation. Tonglu Li: Supervision, Review & Editing. Leandro R. Alejano: Supervision, Project Administration, Investigation, Conceptualization, Writing – Original Draft, Writing – Review & Editing.

Declaration

Conflict of interest: The authors declare that they have no known competing financial interests or personal relationships that could have appeared to influence the work reported in this paper.

References

- Alejano LR (2014) Failure mechanisms on rock slopes and slope stability analysis of simple and complex failures in open pit mines and quarries. Surface Mining Methods, Technology and Systems. Book Chapter. Ed. www.widepublishing.com. Kolkotta, India.
- Alejano LR, Ferrero AM, Ramírez-Oyanguren P, Álvarez Fernández MI (2011) Comparison of limit-equilibrium, numerical and physical models of wall slope stability. International Journal of Rock Mechanics and Mining Sciences 48(1): 16 – 26. <https://doi.org/10.1016/j.ijrmms.2010.06.013>
- Alejano LR, Gómez-Márquez I, Martínez-Alegria R (2010) Analysis of a complex toppling-circular slope failure. Engineering Geology 114(1), 93-104. <https://doi.org/10.1016/j.enggeo.2010.03.005>
- Alejano LR, Veiga M, Gómez-Márquez I, Taboada J (2012) Stability of granite drystone masonry retaining walls: II. Relevant parameters and analytical and numerical studies of real walls. Géotechnique 62(11), 1027-1040. <https://doi.org/10.1680/geot.10.P.113>
- Alejano LR, Veiga M, Pérez-Rey I et al (2019) Analysis of a complex slope failure in a granodiorite quarry bench. Bulletin of Engineering Geology and the Environment 78, 1209–1224. <https://doi.org/10.1007/s10064-017-1160-y>
- Amini M, Ardestani A (2019) Stability analysis of the north-eastern slope of Daralou copper open pit mine against a secondary toppling failure. Engineering Geology 249, 89-101. <https://doi.org/10.1016/j.enggeo.2018.12.022>
- Bar N, Barton N (2024) Q-Slope: Rock Slope Engineering 10 Years on. Rock Mech Rock Eng. <https://doi.org/10.1007/s00603-024-04064-5>
- Barton N, Bandis SC (1990) Review of predictive capabilities of JRC-JCS model in engineering practice. In: Proceedings of the International Symposium on Rock Joints, Barton N & Stephansson O (eds.) Loen, pp 603–610
- Barton N, Choubey V (1977) The shear strength of rock joints in theory and practice. Rock Mechanics 10, 1–54. <https://doi.org/10.1007/BF01261801>
- Bieniawski ZT (1979) The Geomechanics Classification in Rock Engineering Application. Proceedings 4th International Congress on Rock Mechanics, Montreux, 2-8 September 1979, Vol. 2, 41-48.
- Böhme M, Hermanns RL, Oppikofer T et al (2013) Analyzing complex rock slope deformation at Stampa, western Norway, by integrating geomorphology, kinematics and numerical modeling. Engineering Geology 154, 116-130. <https://doi.org/10.1016/j.enggeo.2012.11.016>
- Buergi C, Parriaux C, Franciosi G, Rey J-Ph (1999) Cataclastic rocks in underground structures—terminology and impact on the feasibility of projects. Engineering Geology 51(3), 225-235. [https://doi.org/10.1016/S0013-7952\(97\)00079-3](https://doi.org/10.1016/S0013-7952(97)00079-3)
- Cai M, Kaiser PK, Uno H, Tasaka Y, Minami M (2004) Estimation of rock mass deformation modulus and strength of jointed hard rock masses using the GSI system. International Journal of Rock Mechanics and Mining Sciences 41(1): 3-19. [https://doi.org/10.1016/S1365-1609\(03\)00025-X](https://doi.org/10.1016/S1365-1609(03)00025-X)
- Coulthard MA, Lucas DS, Fuller PG (2004) Application of UDEC to a stress-related mine slope failure at Leigh Creek, South Australia. In: Proc First Int UDEC/3DEC Symp, Bochum, Germany, Rotterdam: Balkema; 2004. pp. 289–96.
- Cui F, Xiong C, Wu Q, et al. (2025) Dynamic mechanism triggering the Catastrophic Xinjing Landslide in Alxa, Inner Mongolia, China. Engineering Geology, 107911. <https://doi.org/10.1016/j.enggeo.2025.107911>

- Dawson EM, Roth RH, Drescher A (1999) Slope stability analysis by strength reduction. *Géotechnique* 49 (1999) 835–840. <http://dx.doi.org/10.1680/geot.1999.49.6.835>
- Ferrus-Piñol B (1994) Structure of As Pontes basin (A Coruña, NW Spain). *Cuadernos Laboratorio Xeolóxico de Laxe*. 19: 73-89.
- Frisch W, Meschede M, Blakey RC (2010) Plate tectonics: Continental drift and mountain building. Springer, 2010. ISBN 978-3540765035
- Gong Y, Yao A, Li Y, Li Y, Li Y, Sun, Y (2023) Model test study on sliding-toppling composite deformation evolution of anti-dip layered rock slope. *Bulletin of Engineering Geology and the Environment*, 82(5), 194. <https://doi.org/10.1007/s10064-023-03213-4>
- González de Vallejo LI, Ferrer M, Ortuño L, Oteo C (2002) Geological Engineering. Ed. Prentice Hall. Madrid.
- Gu D, Huang D (2016) A complex rock topple-rock slide failure of an anacinal rock slope in the Wu Gorge, Yangtze River, China. *Engineering Geology* 208, 165-180. <https://doi.org/10.1016/j.enggeo.2016.04.037>
- Harrison JP, Hudson JA (2000) Engineering Rock Mechanics. Illustrative Worked Examples. Ed. Pergamon Press. London, UK.
- Havaej M, Stead D, Eberhardt E, Fisher BR (2014) Characterization of bi-planar and ploughing failure mechanisms in footwall slopes using numerical modelling. *Engineering Geology*, 178: 109-120. <https://doi.org/10.1016/j.enggeo.2014.06.003>
- Hoek E (2000) Note of the course "Rock Engineering" delivered by the author at UBC, Vancouver (Canadá). Available on the Internet <http://www.rocksience.com>
- Hoek E, Bray JW (1974) Rock Slope Engineering. Institution of Mining and Metallurgy, London
- Hoek E, Carranza-Torres C, Corkum B (2002) Hoek-Brown failure criterion-2002 edition. Proceedings of the 5th North American Rock Mechanics Symposium, Toronto, 7-10 July 2002, 267-273
- ISRM (2007). The Complete ISRM Suggested Methods for Rock Characterization, Testing and Monitoring; 1974–2006. (Resat Ulusay and John A. Hudson eds.). Compilation arranged by the ISRM Turkish National Group, Ankara, Turkey.
- Itasca Consulting Group, Inc. (2019) 3DEC — Three-Dimensional Distinct Element Code, Ver. 7.0. Minneapolis: Itasca.
- Kliche, ChA (1999) Rock Slope Stability. Ed. S.M.E. Society for Mining, Metallurgy and Exploration, Inc. Littleton, Colorado. USA
- León-Buendía C, Santamaría-Arias J, Alejano LR, Giráldez R (2014) Analysis of a complex slope failure in a quartzite slope. *Rock Engineering and Rock Mechanics: Structures in and on Rock Masses - Proceedings of EUROCK 2014, ISRM European Regional Symposium*, pp. 1207-1211. DOI: [10.1201/b16955-209](https://doi.org/10.1201/b16955-209)
- Lo CM, Feng ZY (2014) Deformation characteristics of slate slopes associated with morphology and creep. *Engineering Geology* 178, 132-154. <https://doi.org/10.1016/j.enggeo.2014.06.011>.
- Mohtarami E, Jafari A, Amini M (2014) Stability analysis of slopes against combined circular-toppling failure. *International Journal of Rock Mechanics and Mining Sciences* 67, 43-56. <https://doi.org/10.1016/j.ijrmms.2013.12.020>
- Monge C. (1987) Estudio sedimentológico de la cuenca terciaria de Meirama. Un ejemplo de una cuenca sedimentaria sobre una falla de salto en dirección. *Cuadernos Laboratorio Xeolóxico de Laxe* 11: 51-67.
- Ramírez Oyanguren P, Alejano LR (2008) Rock Mechanics: Fundamentals and Slope Engineering.

International master's degree "Sustainable Use of Mineral Resources". Financed by EU. A
https://www.researchgate.net/publication/281459332_Mecanica_de_Rocas_Fundamentos_e_Ingenieria_de_Taludes_I
Rocscience (2023a) RocPlane: Planar wedge Analysis for Slopes. Rocscience, Toronto, Canada.
Rocscience (2023b) RocTopple: Toppling Stability Analysis. Rocscience, Toronto, Canada.
Rocscience (2023c) Slide2 and Slide 3. 2D & 3D Limit Equilibrium Analysis for Slopes. Rocscience, Toronto, Canada.
Rocscience (2023d) Swedge: Surface Wedge Analysis for Slopes. Rocscience, Toronto, Canada.
Rogers S, Valerio M, Fogel Y et al (2023) Evaluation of inter-ramp scale non-daylighting wedges using a discrete fracture network-based method. 3rd Int. Slope Stability in Min.Conf
Stead D, Eberhardt E (1997) Developments in the analysis of footwall slopes in surface coal mining. Engineering Geology 46(1), 41-61. [https://doi.org/10.1016/S0013-7952\(96\)00084-1](https://doi.org/10.1016/S0013-7952(96)00084-1)
Truzman EM (2009) Metamorphic rock mass characterization using the Geological Strength Index (GSI). In ARMA US Rock Mechanics/Geomechanics Symposium (pp. ARMA-09). ARMA.
Walton G, Atkinson T (1978) Some geotechnical considerations in the planning of surface coal mines. Trans Inst Min Metall Sect A, 87, pp 147-171.
Wei T, Chen G, Zhu Z, Tang P, Yan M (2024) Slope instability mechanism with differential rock mass structure along a fault: a mine landslide from Southwest China. Geomechanics and Geophysics for Geo-Energy and Geo-Resources, 10(1), 76. <https://doi.org/10.1007/s40948-024-00795-5>
Wyllie DC, Mah CW (2004) Rock Slope Engineering: Civil & Mining. 4th Ed. Spon Press. Taylord & Francis Group. London & New York
Xia M, Ren GM, Li TB, Cai M, Yang T J, Wan ZL (2019) Complex rock slope deformation at Laxiwa Hydropower Station, China: background, characterization, and mechanism. Bulletin of Engineering Geology and the Environment, 78(5), 3323-3336. <https://doi.org/10.1007/s10064-018-1371-x>
Yang G, Chen Y, Liu X et al. (2023) Stability analysis of a slope containing water-sensitive mudstone considering different rainfall conditions at an open-pit mine. International Journal of Coal Science and Technology, 10 art. no. 64. <https://doi.org/10.1007/s40789-023-00619-z>
Zhao H, Tian Y, Guo Q, Li M, Wu J (2020) The slope creep law for a soft rock in an open-pit mine in the Gobi region of Xinjiang, China. International Journal of Coal Science and Technology 7(2): 371 – 379. <https://doi.org/10.1007/s40789-020-00305-4>

Combined mechanism failures in rock slopes

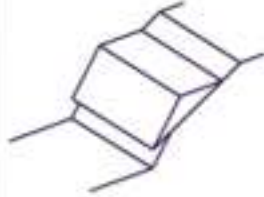

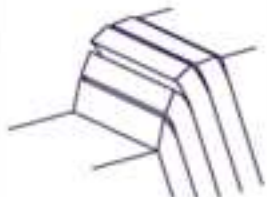



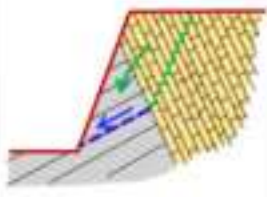



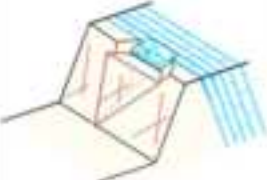


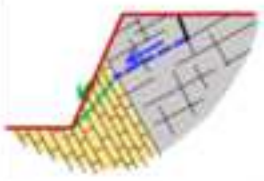
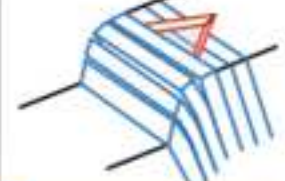
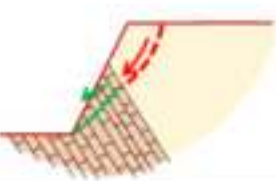

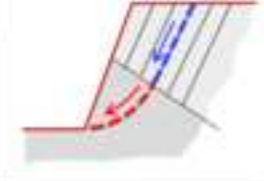
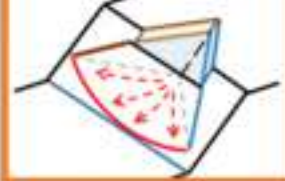
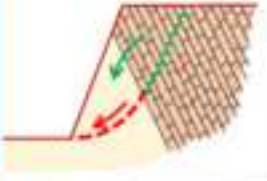
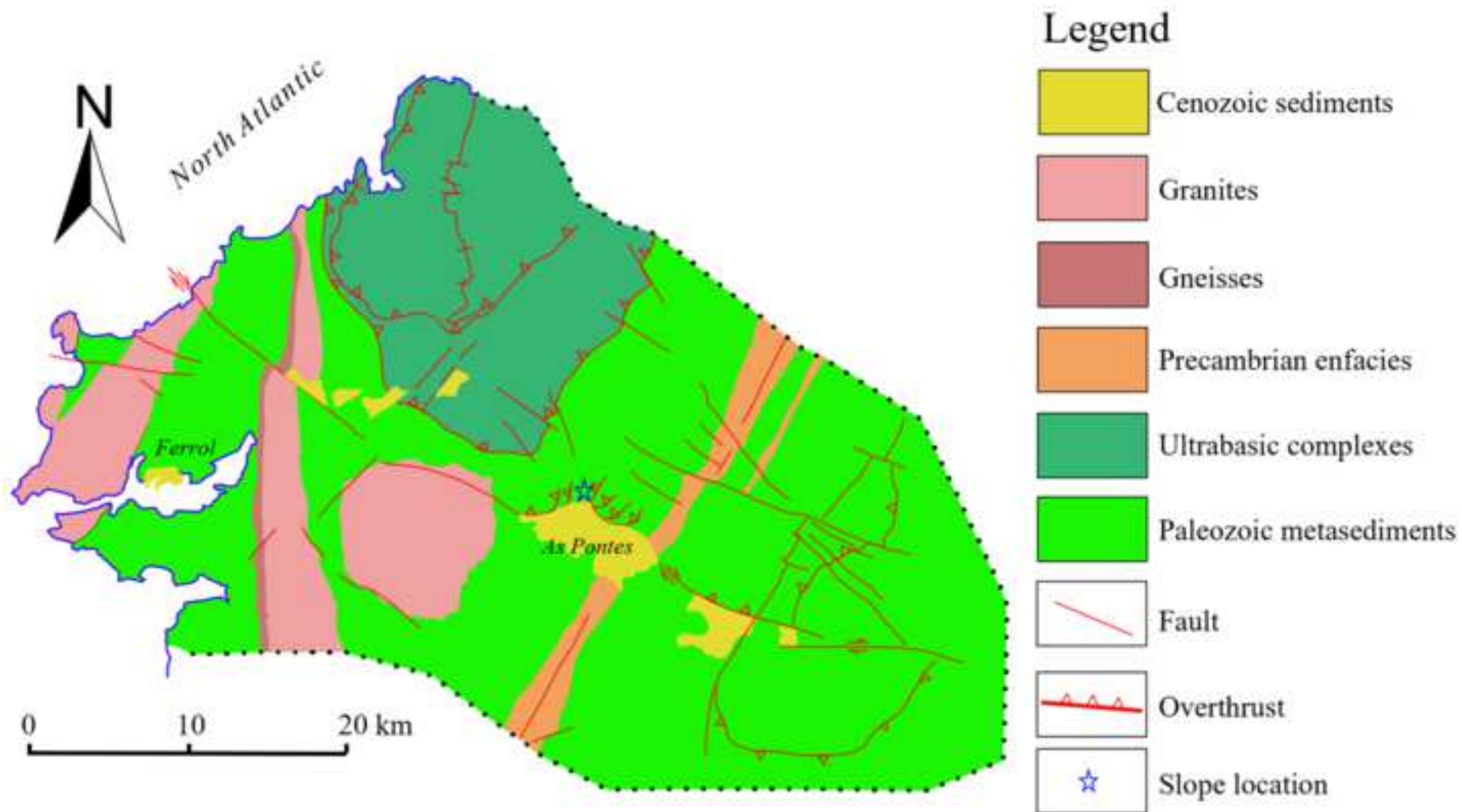
<div>UP</div> <div>DOWN</div>	PLANAR	WEDGE	TOPPLING	CIRCULAR
				
 PLANAR	X	Wedge-Planar 	Toppling-Planar 	Circular-Planar 
 WEDGE	Planar-Wedge 	X	Toppling-Wedge 	Circular-Wedge 
 TOPPLING	Planar-Toppling 	Wedge-Toppling 	X	Circular-Toppling 
 CIRCULAR	Planar-Circular 	Wedge-Circular 	Toppling-Circular 	X

Figure 2



Figure 3



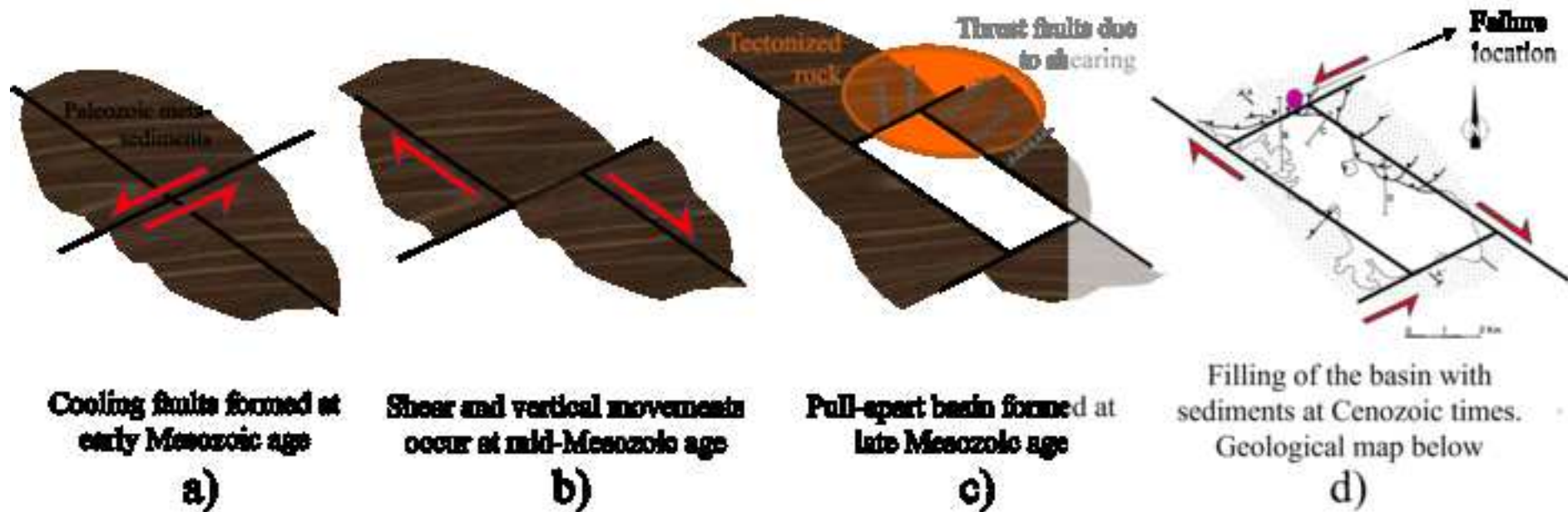


Figure 5

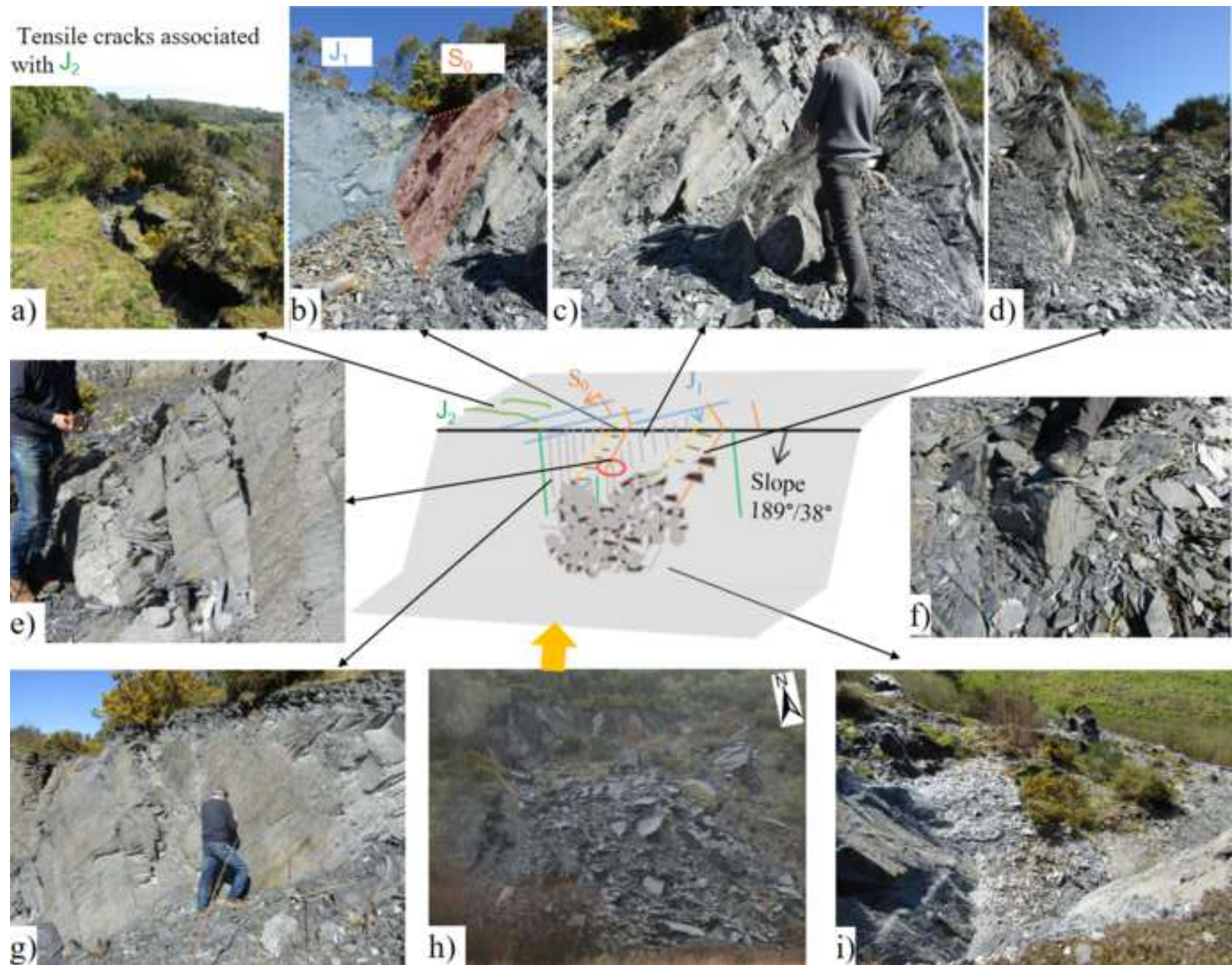
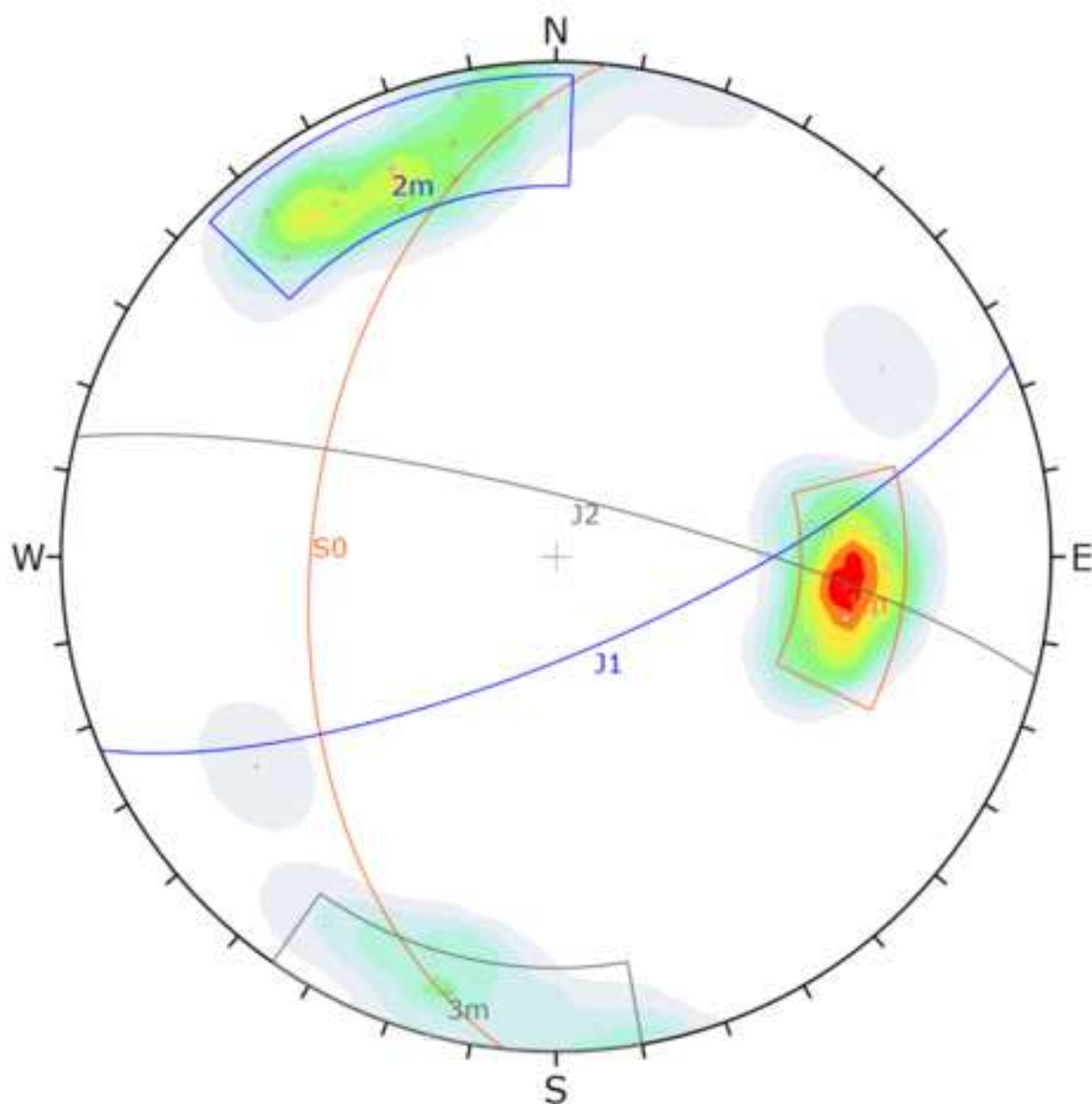


Figure 6

[Click here to access/download;Figure;Fig6.tif](#)

Symbol	Set	Quantity
*	1	8
*	2	9
*	3	5
*	[no data]	2

Color	Density Concentrations
	0.00 - 2.10
	2.10 - 4.20
	4.20 - 6.30
	6.30 - 8.40
	8.40 - 10.50
	10.50 - 12.60
	12.60 - 14.70
	14.70 - 16.80
	16.80 - 18.90
	18.90 - 21.00

Contour Data	Pole Vectors
Maximum Density	20.47%
Contour Distribution	Fisher
Counting Circle Size	1.6%

	Color	Dip	Dip Directio	Label
Mean Set Planes				
1m		49	276	S0
2m		74	157	J1
3m		80	14	J2

Plot Mode	Pole Vectors
Vector Count	24 (24 Entries)
Hemisphere	Lower
Projection	Equal Area

Figure 7

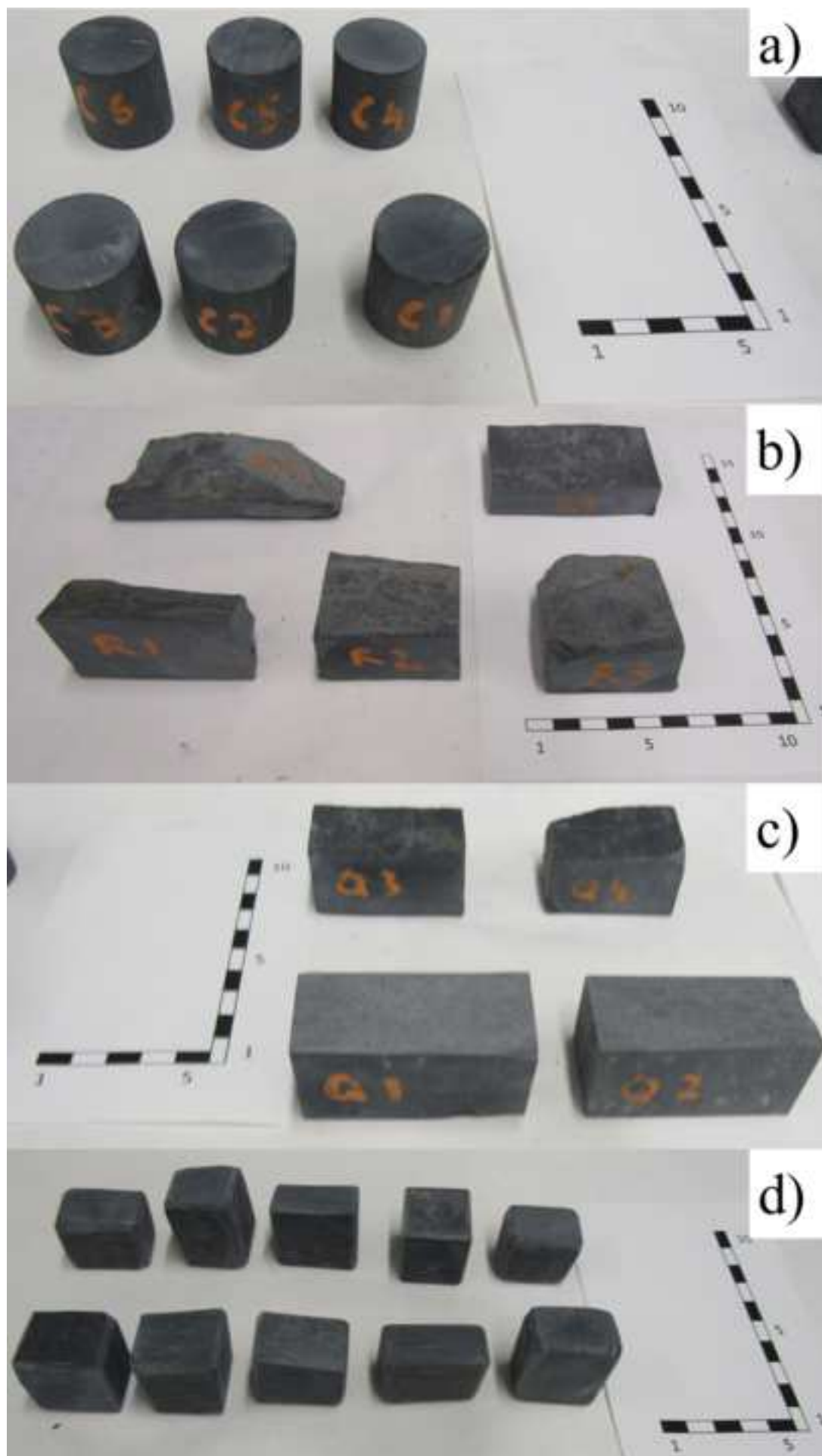
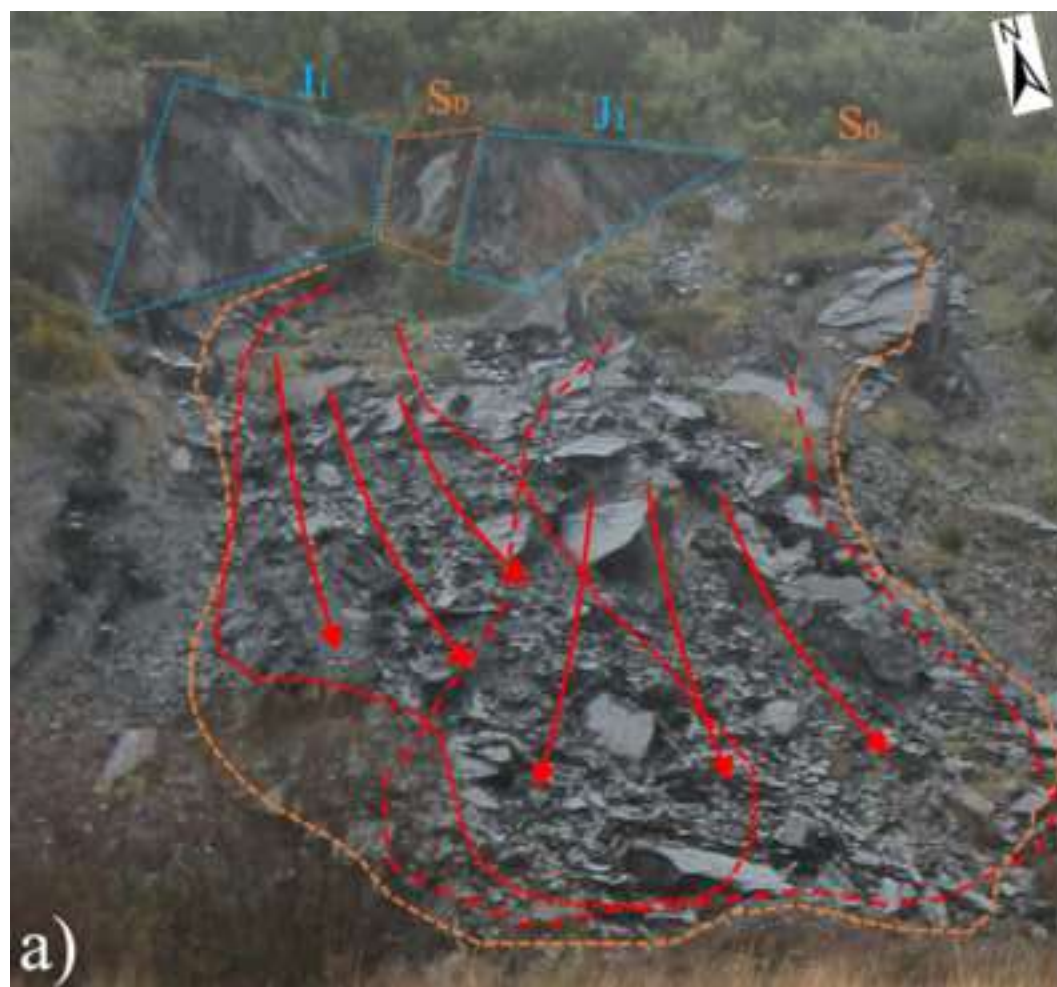


Figure 8

[Click here to access/download;Figure;Fig8.tif](#)



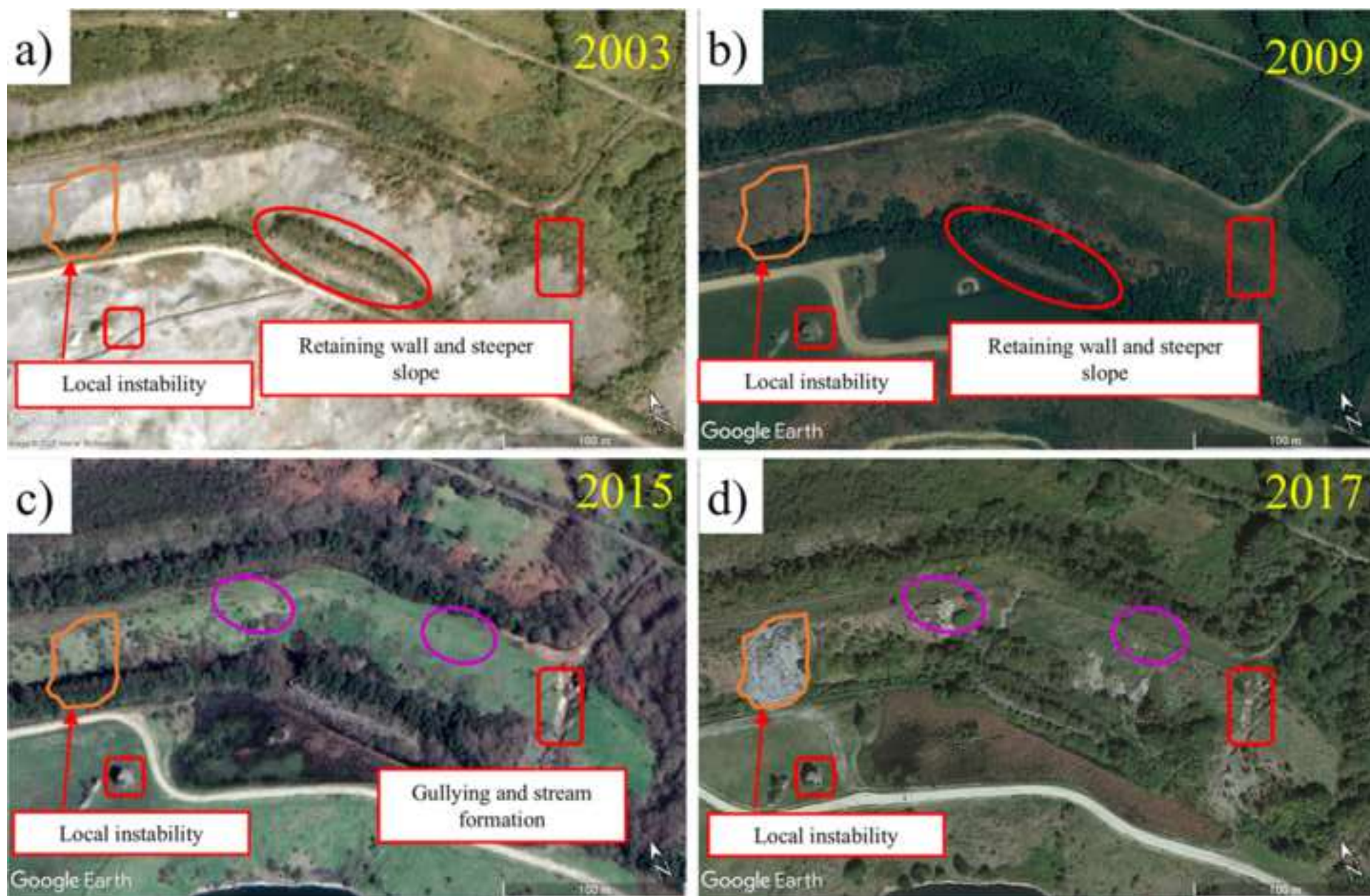
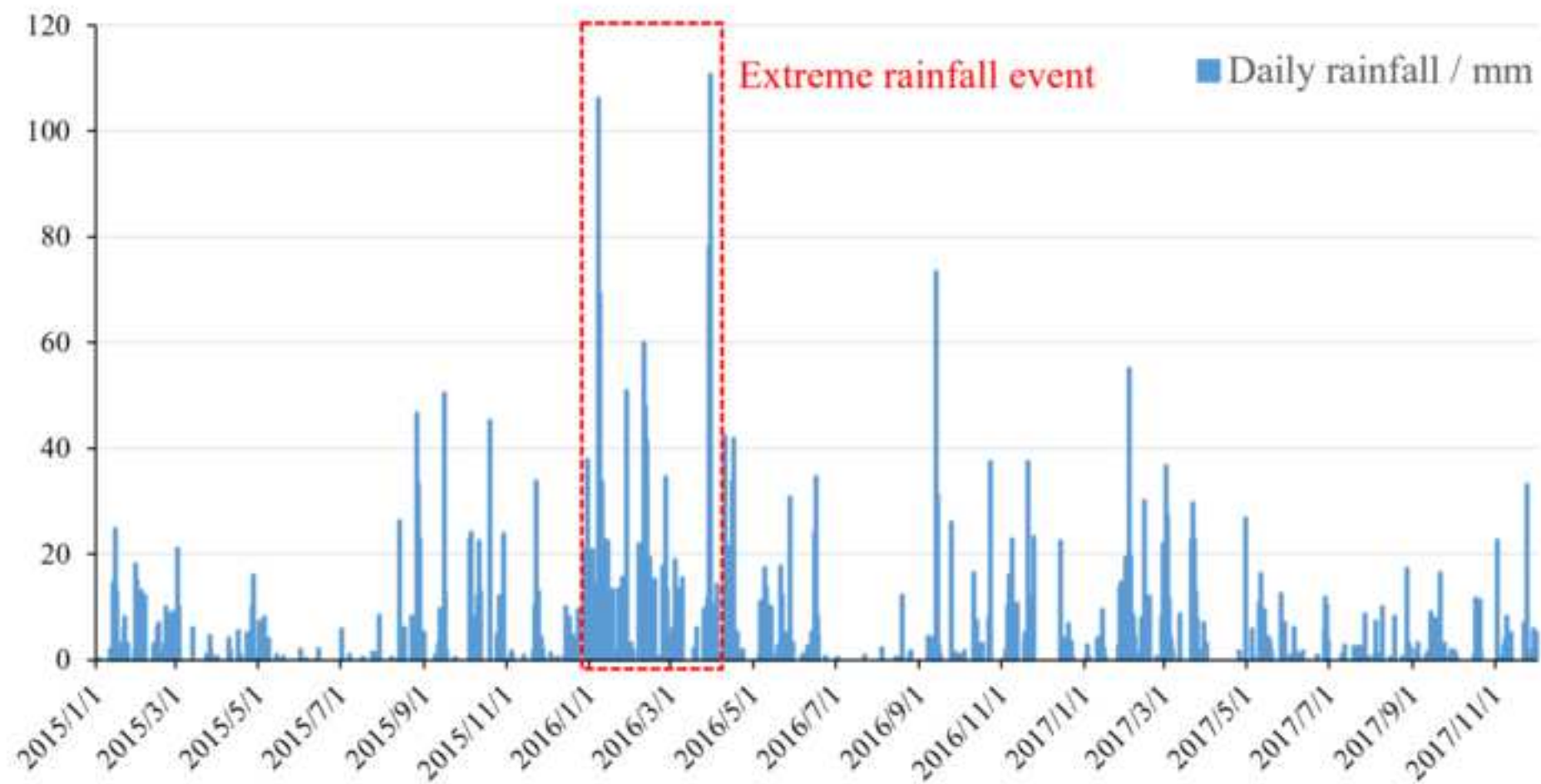
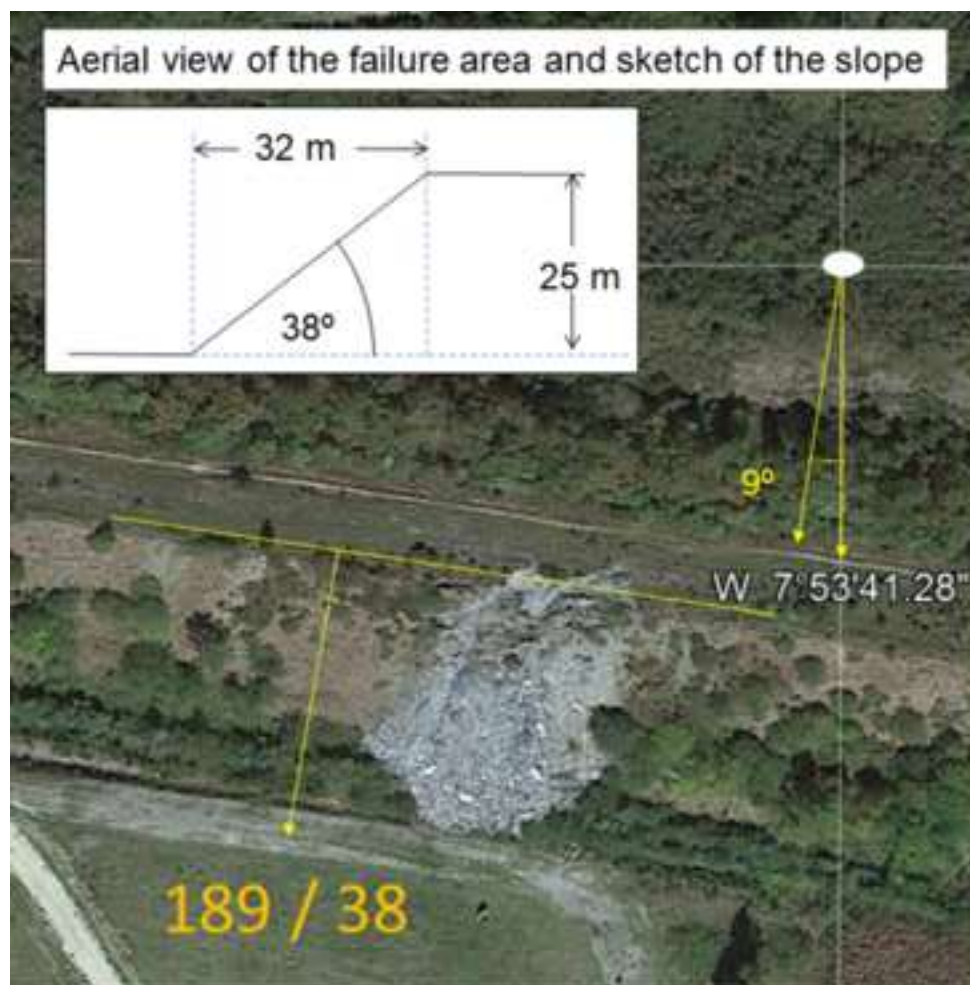
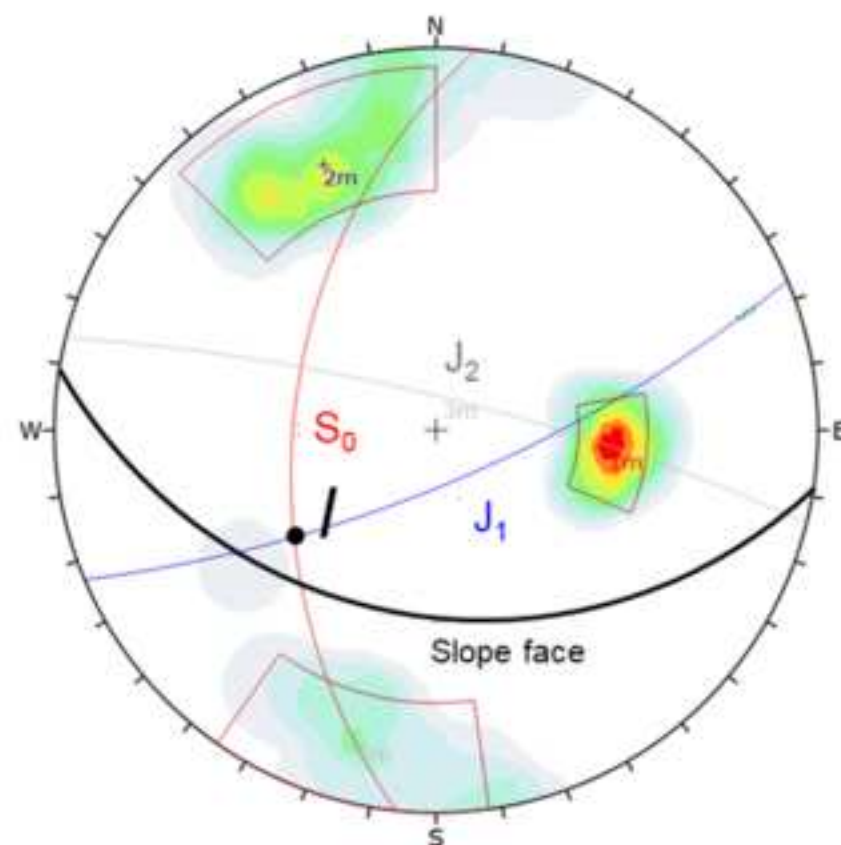


Figure 10

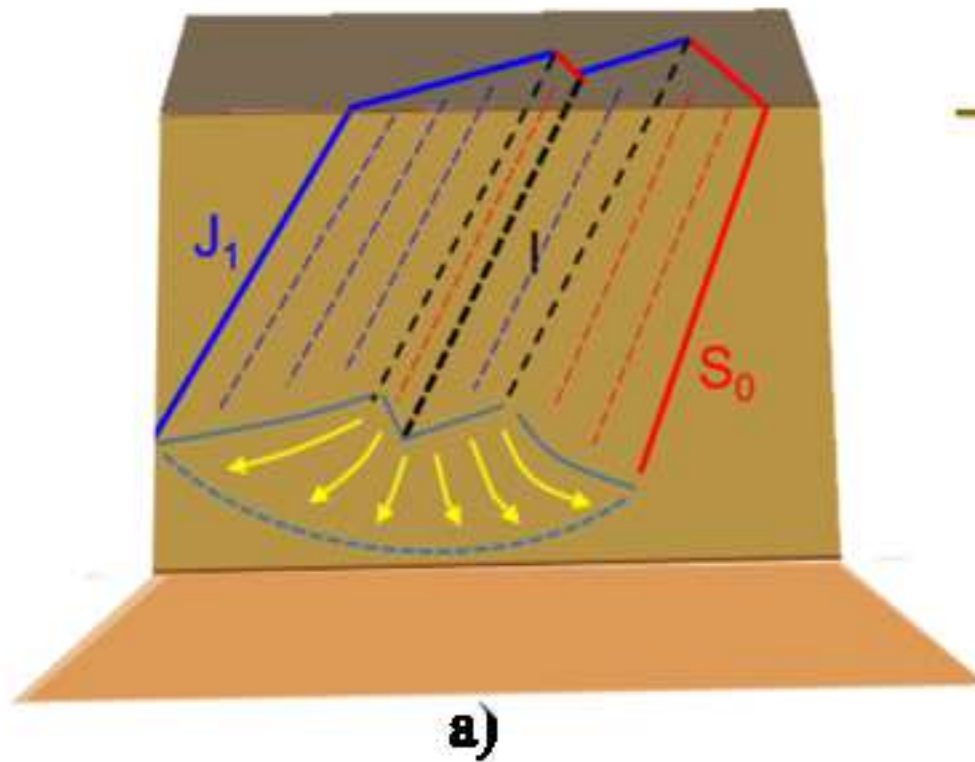




Equal-angle hemispherical stereographic representation of the joint sets identified and the slope face



Front view sketch of the failure mechanism as it was understood by the authors.



Side view of the failure mechanism including sliding in planes J_1 and S_0 forming a double wedge and circular failure in the slope toe.

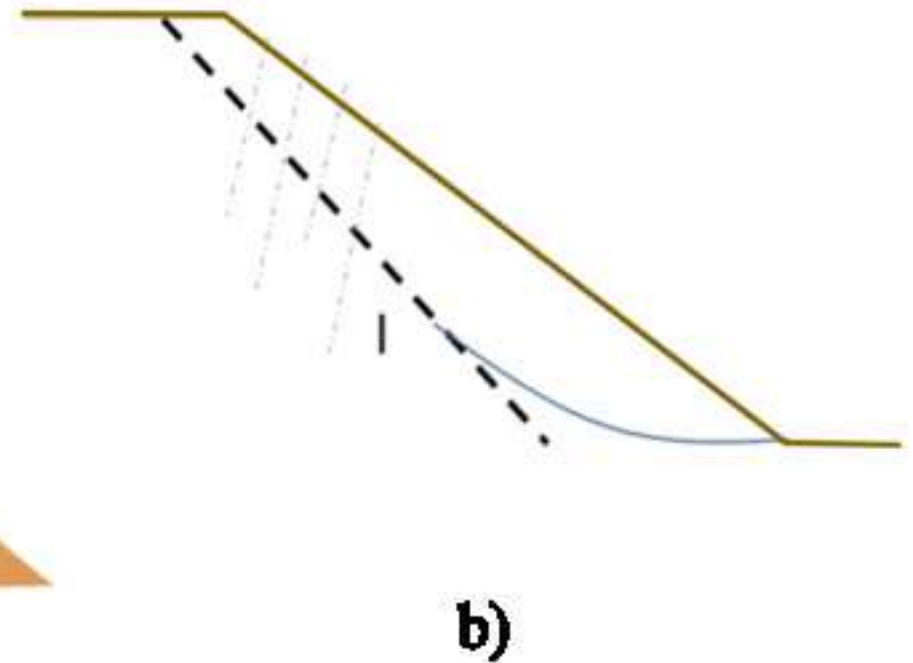
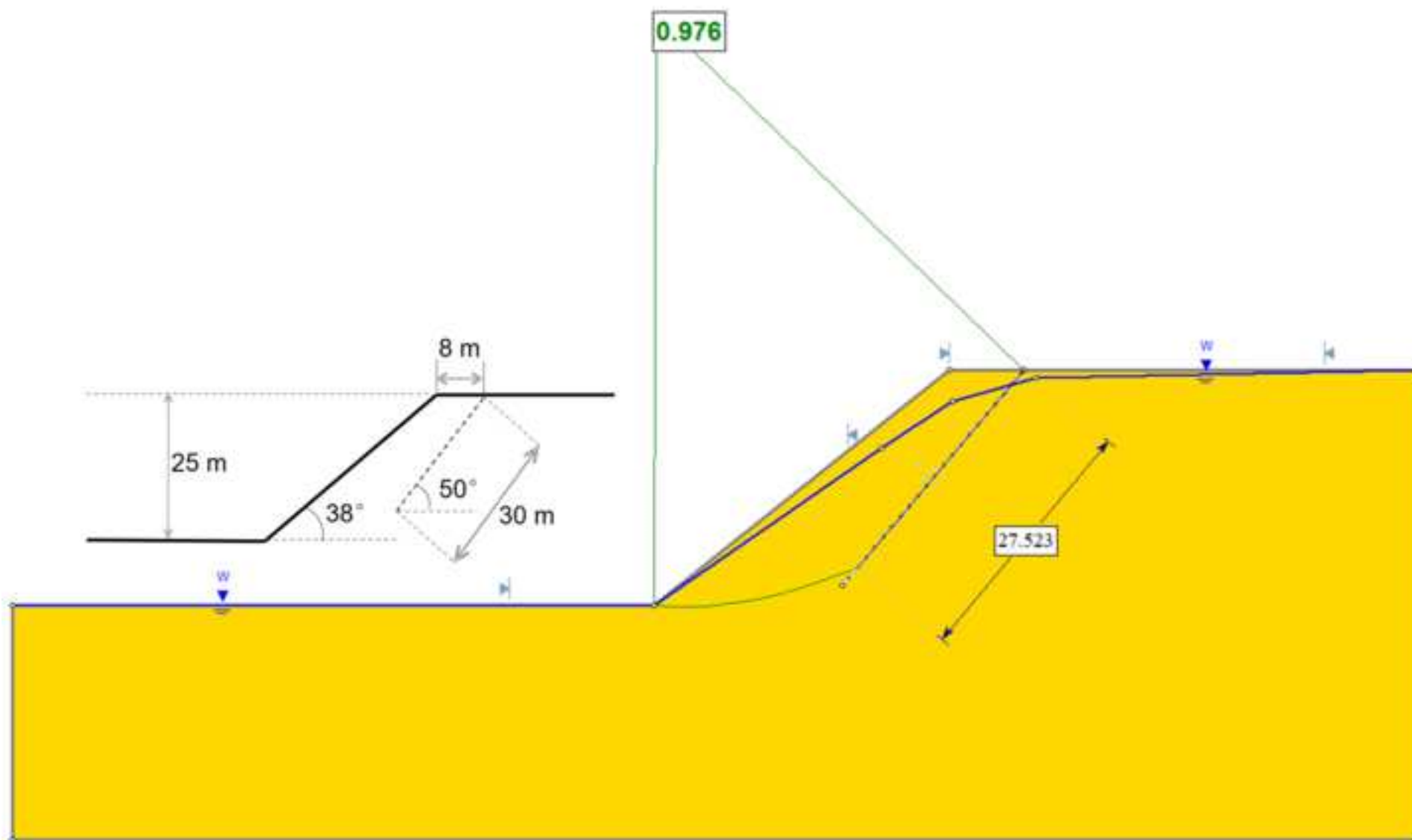
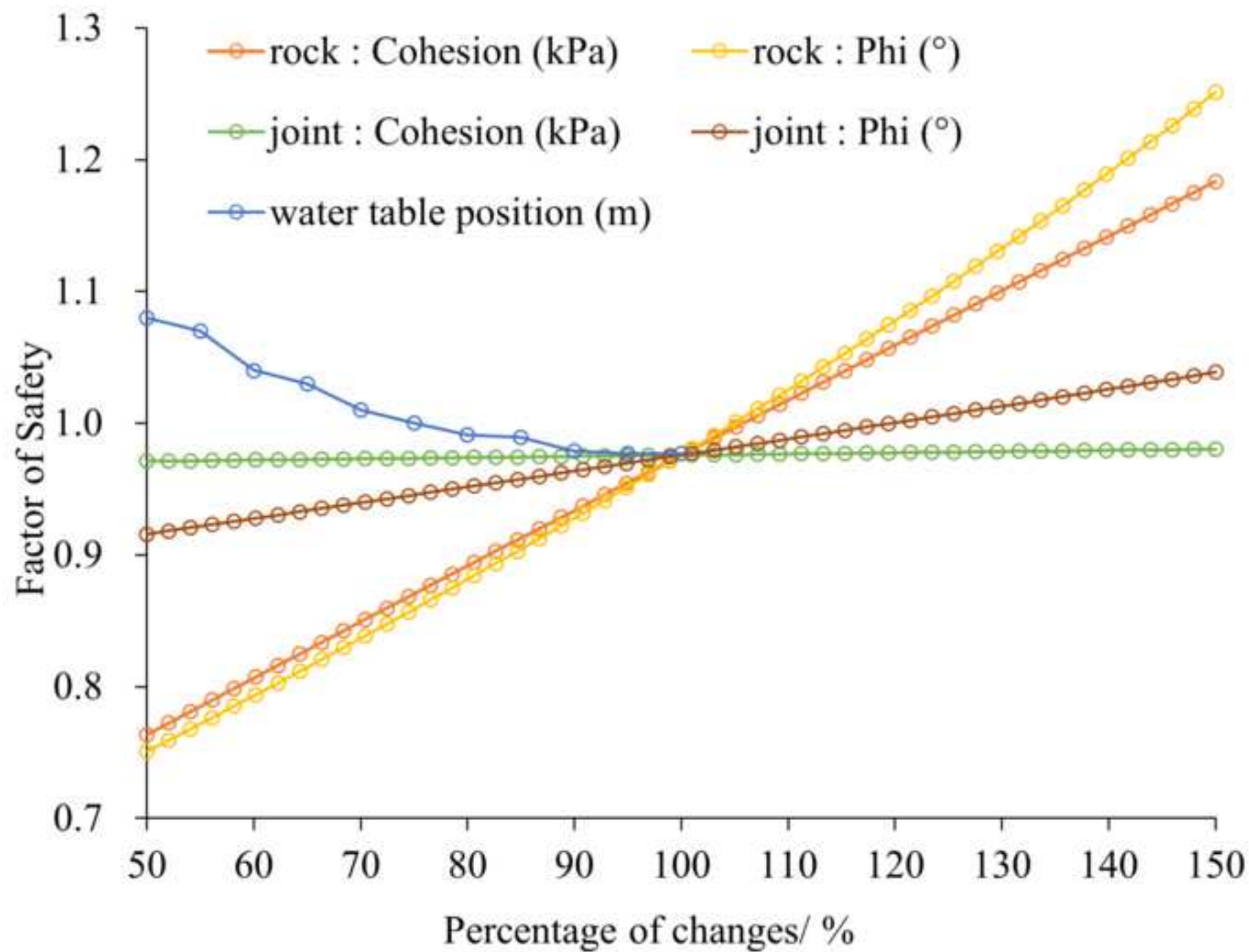


Figure 13





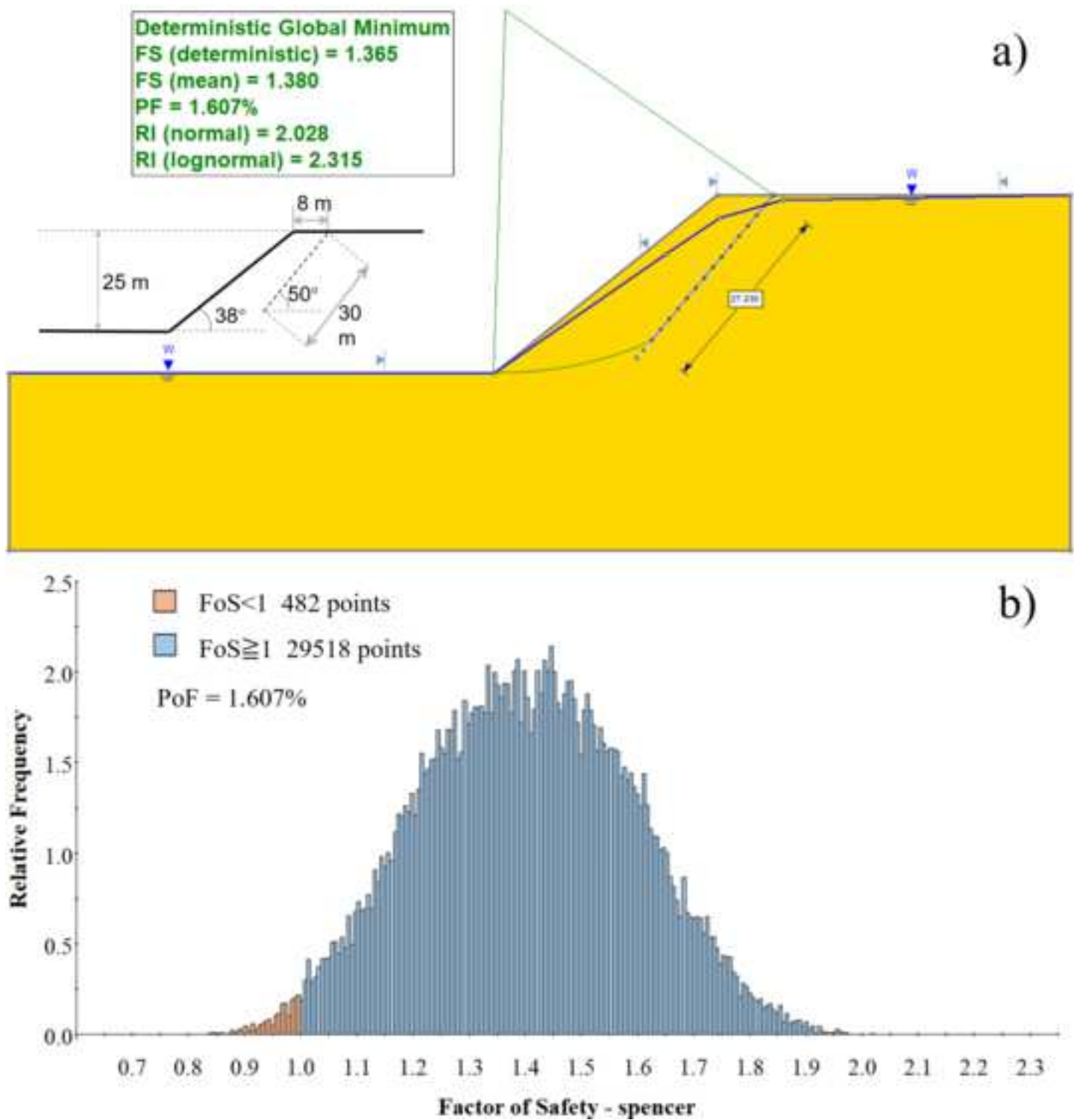


Figure 16

